Trajectories of Middle to Later Stone Age cultural innovation in eastern Africa: the case of Panga ya Saidi, Kenya

Keywords: East Africa, symbolism, ornaments, ochre, bone tools, modern human origin

Abstract

African Middle Stone Age (MSA) populations used pigments, manufactured and wore personal ornaments, made abstract engravings, and produced fully shaped bone tools well before the so-called cognitive shift at 50,000 years ago (ka), formerly considered a key driver in the development of advanced human cultures. However, on-going research across Africa reveals variability in the emergence of cultural innovations in the MSA and their subsequent development through the Later Stone Age (LSA). When present, it appears that cultural innovations manifest regional variability, suggestive of distinct cultural traditions. In eastern Africa, several Late Pleistocene sites have produced evidence for novel activities, but the chronologies of key behavioural innovations remain unclear. The 3 m deep, well-dated, Panga Ya Saidi sequence in eastern Kenya, encompassing 19 layers covering a time span of 78 ka beginning in late MIS 5, is the only known African site recording the interplay between cultural and ecological diversity in a coastal forested environment. Excavations have yielded worked and incised bones, ostrich egg shell beads, marine shell beads, worked and engraved ochre pieces, fragments of coral, and a belemnite fossil. Here we provide a detailed analysis of this material. We demonstrate that behavioural modernity on the eastern African coast is evident by 67 ka, and exhibits remarkable diversity and innovation through the LSA and Iron Age. We suggest the cultural trajectories evident at Panga ya Saidi were shaped by both regional traditions and cultural/demic diffusion.

Introduction

The present study aims to document the emergence of key behavioural innovations in the late Middle Stone Age (MSA) and the Later Stone Age (LSA) of eastern Africa. The emergence of innovations such as the use of mineral pigments, the wearing of ornaments and the production of abstract engravings has traditionally been interpreted as the direct consequence of cognitive changes linked to the origin of our species in Africa (McBrearty and Brooks, 2000; Henshilwood and Marean, 2003; Shea, 2011; Bruner, 2014; Marean, 2015; Coolidge and Wynn, 2017, Rito et al., 2019). A significant debate crosscutting archaeology, palaeoanthropology and archaeogenetics has persisted over whether cultural modernity originated and spread uniquely with anatomically modern *Homo sapiens* (Stringer and Andrews, 1989; Relethford and Harpending, 1994; Klein, 1995; Agani et al., 2011; Henn et al., 2012; see Rito et al., 2019 for an update of this view) or whether it emerged in the context of biological and cultural interactions between diverse hominid populations in disparate climatic and geographic settings (Gunz et al., 2009; Hublin et al., 2017; Neubauer et al., 2018; Scerri et al., 2018).

Resolving these issues is critically important for understanding the biological and genomic origins of our species. Unfortunately, the archaeological record for manifestations of hominid symbolism and "modern" innovations remains poorly resolved overall. Current models are shaped by the higher resolution records from Europe (d'Errico and Banks, 2015; Locht et al., 2016; Giaccio et al., 2017; Zilhão et al., 2017) and increasingly southern and northern Africa (Jacobs et al., 2008; Jacobs et al., 2011; Jacobs and Robert 2015; d'Errico et al., 2018). Eastern Africa -one of the assumed centers of human cultural and biological evolution- is represented by only a handful of sites with artifacts indicative of symbolic-mediated behavior and complex bone technology (Ambrose, 1998; Assefa et al., 2008, 2018; Miller and Willoughby, 2014; Rosso et al., 2014, 2016, 2017; Brooks et al., 2018). Most of these have lacked systematic analysis until only very recently (Brooks et al., 2018; Tryon et al., 2018; Miller, 2019). These records are biased toward the Central Rift Valley of the interior, which may not reflect the full diversity of behaviours across the landscape. A greater limitation is that many of these important assemblages lack the chrono-spatial resolution to accurately gauge change over time, are not associated with local climatic data, and/or are not associated with the remains of their hominid creators. As a result, we can assemble a chronology for changes in human symbolism in the region but we lack the data linkages needed to test aforementioned hypotheses regarding the drivers for the emergence of symbolism and symbolic change through time.

Panga ya Saidi, a recently published archaeological sequence located north of Mombasa in Kenya, and spanning the last 78 ka (Shipton et al., 2018), has yielded a large collection of personal ornaments, bone artifacts, modified ochre and engraved objects spanning the MSA/LSA transition in a continuous sequence that extends into the late Iron Age of recent centuries. This sequence of symbolic behaviours is well-dated, linked with a high-resolution palaeoecological record and rich technological assemblages (Shipton et al., 2018), and contains human burials that have yielded ancient DNA (Skoglund et al., 2017). Panga ya Saidi is also the only site where systematic flotation and fine mesh screening permitted high rates of recovery for small symbolic artifacts. As a result, the site offers a unique insight into the emergence of key cultural innovations in eastern Africa. We characterize these innovations with the aim of identifying regional trends and similarities with innovations recorded in neighbouring regions, proposing hypotheses regarding the impact of these innovations on late MSA and early LSA eastern African societies, and discussing the implication of this record for our understanding of the emergence of behaviourally modern human cultures.

Background

The complex and non-linear patterns emerging from our current state of research highlights the need to expand symbolic datasets within Africa. Artifacts that suggest symbolic practices (e.g., pigments, ornaments, burials, abstract engravings and drawings, systems of notation) appear at different times in Africa and some of them are still not found in vast areas of this continent until a few thousand years ago. Moreover, some of these innovations seem to disappear for thousands of years and then reappear in other forms, contradicting the idea of an exponential expansion of symbolic material culture linked to the sudden origin of new cognitive abilities.

The use of mineral pigments is the only innovation that coincides, to a degree, with the beginning of the Middle Stone Age. The recent discovery of modified red ochre fragments at Olorgesailie, Kenya (Brooks et al., 2018) confirms previous discoveries of modified ochre in the early MSA made at Kapturin in Kenya, Twin Rivers in Zambia, and Wonderwerk, Canteen Kopje and Kathu Pan 1 in South Africa (Barham, 2002; Watts et al., 2016). However, considering the age of these findings, 320-280 ka for Olorgesailie and earlier for the southern Africa sites, and what we know about the anatomy of the contemporary African human populations, the first users of ochre pigments probably possessed a number of archaic morphological attributes. Therefore, the first pigment use cannot be taken as reflecting the emergence of modern culture triggered by a speciation event. The first known ornaments, consisting of perforated marine gastropods covered with ochre, belonging to the species *Tritia gibbosula*, are found at sites in Morocco and Algeria dating back to between 120 ka and 80 ka (Bouzouggar et al., 2007; d'Errico et al., 2009; Steele et al., 2019). Perforated shells belonging to the same species and bivalves of the genus *Glicymeris*, found at Qafzeh and Skhul, in the Near East, date back to about the same period (Mayer et al., 2009). *Afrolittorina africana* and *Mancinella capensis* shells are used as beads at Sibudu, Kwa-Zulu Natal, in layers dated to between 70 ka and 46 ka (d'Errico et al., 2008; Vanhaeren et al., in press). Perforated and ochred marine gastropods, belonging to the species *Nassarius kraussianus*, are used as ornaments at Blombos Cave, Eastern Cape, around 73 ka (d'Errico et al., 2005). At Border Cave, Kwa-Zulu Natal, a whole *Conus ebraeus* that was perforated and ochred was found in a pit dated to 74 ka, in which the body of an infant was deposited (d'Errico and Backwell, 2016).

Abstract representations, engraved on bone and ochre pieces, or drawn with ochre pencils on stone, are found at Blombos Cave, Klasies River, Klein Kliphuis, Sibudu, and Pinnacle Point, South Africa, where they date to between ca. 100-70 ka (Mackay and Welz, 2008; Henshilwood et al., 2009, Watts, 2010; d'Errico et al., 2012). They disappear in the following period and reappear in the same region, but engraved on ostrich egg shells used as flasks for water, ~66-58 ka (Texier et al., 2013; Henshilwood et al., 2014), and later on *Achatina* shells (Bicho et al., 2018) and bone (d'Errico et al., 2012). Abstract representations disappear later and are not found again at African sites until a few thousand years ago. The first African figurative art, discovered in the Apollo 11 cave in Namibia, is only 30,000 years old (Wendt, 1975; Rifkin et al., 2015). Although the subject of bitter discussion (Val, 2016; Dirks et al., 2016), the first African mortuary practices could be associated not with modern humans but with a population of *Homo naledi*. Discovered at the bottom of the cave of Rising Star in South Africa, this hominin with a small cranial volume may have survived until between 226 ka and 335 ka (Dirks et al., 2017; Hawks et al., 2017). The very few primary burials discovered on this continent are younger than burials of Neanderthals and modern humans found outside Africa (Pettitt, 2010).

What makes it difficult to interpret the first examples of complex technologies and symbolic behaviours from Africa as the direct consequence of a geographically and chronologically constrained emergence of our species is the fact that comparable cultural manifestations are now known in Eurasia before the arrival of modern populations in those regions (e.g., Roebroeks and Villa, 2011; Joordens et al., 2015; Jaubert et al., 2016; Majkic et al., 2017; d'Errico et al., 2018; Hofmann et al., 2018). In other words, the innovations that we encounter at archaeological sites and in which we recognize the first traces of a cognition similar to ours, in particular symbolic manifestations, do not appear to be the direct result of a change related to the sudden emergence of a modern anatomy but rather the expression of complex and apparently non-linear cultural trajectories (Johansson, 2015; Acherman et al., 2016; d'Errico et al., 2017; Colagé and d'Errico, 2018; d'Errico and Colagé 2018; Dediu and Levinson, 2018; Kissel and Fuentes, 2018; Scerri et al., 2018; Will et al., 2019). How these trajectories were, in different regions on the planet, conditioned by biological, environmental, and social factors as well as by migrations and diffusion of cultural traits remains to be explored.

The MSA to LSA transition in eastern Africa is marked by the development and proliferation of disk beads, particularly those made from ostrich egg shell (OES). At present, eastern Africa has yielded the earliest occurrences of OES beads, with specimens directly dated to ca. 52,000 BP at Mumba Rockshelter in Tanzania (Gliganic et al., 2012), >50,000 years BP at Magubike Rockshelter in southern Tanzania (Miller and Willoughby 2014), 40,600 BP at Kisese II in central Tanzania (Tryon et al., 2018), and 39,900 BP at Enkapune ya Muto in southern Kenya (Ambrose, 1998). Variation in OES bead representation, size, and morphology through time and space has itself been the source of considerable debate in the Pleistocene through to the Iron Age. While bead sizes seem to generally decrease through the Pleistocene and early Holocene in southern Africa (Miller, 2019), sites in eastern Africa appear to show more heterogeneous patterns. Whereas most sites in the interior appear to show little overall change through time (Miller, 2012; Miller and Willoughby, 2014; Biitner et al., 2017), Tryon et al. (2018) report a slight reduction in disk bead dimensions through the sequence at Kisese II. In southern Africa, a sudden shift to larger bead sizes in the Late Holocene is thought to correspond to the arrival of new populations of herders with different stylistic preferences. So far, there is very little data on any possible shifts in bead size through dynamic population changes now demonstrated through archaeogenetics for the Mid-to-Late Holocene of this region (Skoglund et al., 2017; Prendergast et al., 2019). There are also few indications of periods of intensification of symbolic behaviors that may lend clues to the forces affecting their initial emergence.

Bone tools are even less well studied in eastern Africa. The bone tool and notational/ornamental assemblages documented in the MSA of southern Africa (d'Errico and Henshilwood, 2007; Blackwell et al., 2008; d'Errico et al., 2018) and possibly Central Africa (Brooks et al., 1995; Yellen et al., 1995) have no equivalent in eastern Africa. Bone implements first appear *en masse* in eastern Africa in the form of barbed bone points or "harpoons" associated with aquatic resource intensification by foragers during the wet phase of the early Holocene (Yellen, 1998). Similarly, widespread bone ornament traditions are not visible until the Mid-to-Late Holocene (Mehlman, 1989; Helm, 2000; Langley et al., 2017). However, descriptions of five un-serrated bone projectile points, a bone awl, and a bone notched piece from Kuumbi Cave on the Zanzibar archipelago of Tanzania hints at earlier manifestations of osseous technologies on the eastern African coast (Langley et al., 2016).

Material and methods

Archaeological and paleoecological context

Panga ya Saidi is a large, partially unroofed cave complex located on the Nyali Coast of Kenya, 15 km from the present-day shore, at an altitude of 150 m (Figure 1). It opens on the eastern flanks of the Dzitsoni Uplands, a ridge of Middle Jurassic limestone that separates the Late Quaternary coastal plains from the large, arid Nyika Plateau. The site remained in close proximity to the coast throughout the Upper Pleistocene since the sea depth at -125 m is within 5 km of the present shore line. Ecologically, the Dzitsoni Uplands vegetation belongs to the Zanzibar-Inhambane Regional Mosaic. The site is situated at the limit between the Sokoke Forest, characterised by the association *Cynometra-Manilkara* and the Shale Savanna with *Manilkara-Dalbergia*. Climate models (Shipton et al., 2018) suggest that during the Last Interglacial the Nyika Plateau received less rainfall than the present interglacial, while the coastal area where the site is located witnessed higher precipitation in the Last Glacial Maximum than at present.

Excavations conducted at Panga ya Saidi between 2010 and 2013 have reached a depth of 3 m (Shipton et al., 2018). The sequence includes, from the bottom to the top, four lithological units (Units I-IV) encompassing 19 archaeological layers (Figure 2). Although animal burrows, tree root channels and termite galleries were recorded during the excavations, most stratigraphic boundaries could be identified along the entire profile. Twelve stratigraphically coherent AMS radiocarbon and seven OSL ages indicate that the sequence accumulated between MIS 5 (~ 78 ka) and the historical era (0.4 ka). Unit I (Layers 19-17), featuring a relatively low occupation density, is followed, at the Unit I/II interface (Layer 17/16) by a possible depositional hiatus and limited human use of at least the part of the cave sampled. Anthropogenic signatures, in the form of ash and burnt bone, gradually increase within Unit II (Layers 16 to 14). This trend is interrupted by a sharp surface of erosional relief separating the top of this unit from the archaeologically richer Unit III (Layers 13 to 5). This unit comprises numerous ash lenses interpreted as burning features. Stratigraphic interfaces interpreted as occupation surfaces with some degree of erosion are identified within Unit III, in particular at the Layer 13/12 and Layer 10/9 boundaries. The overall sequence is as follows: Layers 1-3 (Iron Age), Layer 4 (earlier Holocene), Layers 5-6 (terminal Pleistocene), Layers 7-8 (Last Glacial Maximum), Layer 9 (late MIS 3), Layer 10 (mid-MIS 3), Layers 11-12 (early MIS 3), Layers 13-16 (MIS 4), and Layers 17-19 (late MIS 5). A range of palaeoecological indicators identify a persistence of more or less open tropical forest throughout the sequence. Within this general trend, several proxies suggest slightly drier conditions during the deposition of Layers 16 (71-67 ka) to 8 (20 ka).

A significant increase in archaeological finds and a change in stone artifact size, technology, raw material and tool type are recorded after the Unit I - II transition (73-67 ka). Lithic assemblages from Unit I are primarily composed of typical MSA large flakes, mostly made of limestone, produced with the Levallois method, occasionally retouched into points. The shift to a largely predominant use of quartz (70-90%) in Units II and III corresponds to an increased use of bipolar technology and a reduction in stone tool size. Chert use increases (40-60%) in Unit IV. Backed crescents appear for the first time in Layers 11 and 12 (48.5 ka) and are also found from Layer 6 upwards. They co-exist in Units II and IV with bipolar and Levallois technology, with blades becoming common in the upper part of the sequence (Layers 8–3; 25–1 ka). The increase in archaeological remains observed in Units II-IV is tentatively interpreted by Shipton and colleagues (2018) as evidence for a growing human presence in the region, while the absence of unidirectional changes in lithic technology is seen as an indication that this region did not witness the sudden appearance of an LSA technological package.

Methods

Over 200 potential beads, bone tools, engraved bone and stone objects, and pigment lumps recovered during excavations were examined under a low power reflected light microscope to assess potential anthropogenic modifications. When necessary, sediment was carefully removed under the microscope with a soft brush or a wet toothpick. This resulted in the retention of 180 pieces bearing compelling traces of manufacture and use, unmodified or marginally modified shell fragments probably used as beads, and modified and unmodified lumps of iron-rich rocks and sediments, possibly used to produce ochre powder.

The identification of the most probable ostrich sub-species that laid the eggs used to produce the circular beads found at Panga ya Saidi was based on guidelines proposed by Schönwetter (1927), Sauer (1972), Mourer-Chauviré and Geraads (2008), and Blinkhorn et al. (2014). Taphonomic analysis of *Conus* shells was based on Harding (1961), Mattes (1974), Claassen (1998), and d'Errico and Backwell (2016). The identification of traces of manufacture, heating and use-wear on beads made from marine shells and OES relied on diagnostic criteria established experimentally (d'Errico et al., 1993; d'Errico et al., 2005; d'Errico et al., 2009), as well as previous analyses of similar objects (Kandel and Conard, 2005; Orton, 2008; d'Errico et al., 2012; Wei et al., 2017).

The distinction between natural and anthropogenic modifications on worked bone was based on criteria defined in the literature and on the analysis of modern and Pleistocene reference collections (Binford, 1981; Bonnichsen and Sorg, 1989; Villa and d'Errico, 2001; Backwell and d'Errico, 2001, 2005). Identification of shaping techniques and use-wear was based on data from experimental bone tool manufacture and use (Newcomer, 1974; d'Errico et al., 1984; Bergman, 1987; Shipman and Rose, 1988; Choyke and Bartosiewicz, 2001; Backwell and d'Errico, 2005), and experimental reproduction and microscopic analysis of marks produced with different tools and motions (d'Errico, 1995, 1998).

The identification of grinding, scraping and traces of deliberate engraving on ochre fragments is based on criteria obtained from experimental research (d'Errico and Nowell, 2000; Soressi and d'Errico, 2007; Hodgskiss 2010; Rifkin, 2012; Rosso et al., 2017), examinations of engravings on stone and bone surfaces (d'Errico, 1995, 1996), and by comparison with published engraved pieces from Blombos Cave and Klasies River (Henshilwood et al., 2002, 2009; d'Errico et al., 2012).

Two to four sides of each artifact were digitised at a resolution of 2400 dpi with an Epson Perfection V600 Photo scanner. Artifacts were examined at magnifications between 4x and 40x, and photographed with a motorised Leica Z6 APOA microscope equipped with a DFC420 digital camera. Uploaded images were treated with Leica Application Suite (LAS) equipped with the Multifocus module, and Leica Map DCM 3D computer software. Selected areas of one *Conus* were scanned using a Sensofar Sneox scanning confocal microscope using a 20x objective. The resulting files were analysed with Mountains 7.2 software.

Different variables were recorded for each artifact category. Morphometric data were collected on all objects with digital callipers. On shaped beads, we recorded raw material, bead shape, colour, traces of manufacture, perforation technique, traces of heating, morphology of the perforation (sub-conical, biconical, cylindrical and sub-cylindrical), the hole (circular, sub-circular, ovoid), and the hole aperture at the level of the bead surface, presence of pigment residues, and thickness and maximum and minimum diameter of the bead, the hole and the aperture. Identification of OES bead types, corresponding to different size, technology and style of manufacture, has taken advantage of discussions with Gwaxan Cgonta, an OES beads maker and member of the Ju/'hoansi community, Nyae Nyae, near Tsumkwe, Namibia, as well as analysis of OES beads from Shuidonggou locality 2 (Wei et al., 2017). On anthropogenic perforated marine gastropods, we recorded species, shell length, width, maximum and minimum diameter of the perforation, perforation technique, and traces of shaping and use-wear. On naturally perforated or slightly modified spiral fragments of *Conus*, we recorded, if any, location and type of modification, maximum width and thickness of the fragment, and perforation maximum diameter. The raw material from which four shaped beads, tentatively identified in the field as made of "shale" or "slate", was manufactured, was assessed by optical microscopy and micro-Raman spectrometry (μ-RS). We used for this purpose a SENTERRA Dispersive Raman Microscope (Bruker), equipped with an internal calibration system. Spectra acquisitions were done with a 532 nm laser, a laser power of 2 mW, an integration time of 60 s, and multiple co-additions. The working area was observed through the integrated colour camera, and data was collected with the software package OPUS 7.2. Identification of mineral phases was based on the comparison of the recorded spectra with those of the RRUFF spectra library (Lafuente et al., 2015).

The following parameters were recorded, wherever possible, on worked bone and teeth: anatomical and species origin of the blank, mammal size class, blank extraction and shaping technique, traces of use, sharpening, and the length, width and thickness of the object. The location and extent of worked areas and the sequence of the technical actions, based on microscopic examination, were systematically recorded for each artifact.

Variables recorded on iron-rich lumps included type and location of anthropogenic modification, colour, and texture. The elemental composition of two modified iron-rich lumps was established by energy dispersive X-ray fluorescence (EDXRF) and analysis using a scanning electron microscope coupled to an energy dispersive spectrometer (SEM-EDS). The former was not used on unmodified lumps because of their small size. EDXRF measurements were performed with a portable SPECTRO xSORT X-ray fluorescence spectrometer from Ametek, equipped with a silicon drift detector (SDD), a low power W X-ray tube with an excitation source of 40 kV, and an X-ray beam of 8 mm. Spectra acquisition times were set to 300 s. The spectrometer is internally calibrated by an automated measure of the elemental composition of a standard metal shutter. Measurements were acquired using a positioning device consisting of a lead receptacle to which the spectrometer was fixed. Three measurements per object were obtained. SEM-EDS analyses were performed using a FEI Quanta 200 with SiLi detector, and SDD-EDAX detector. Backscattered electron images (BSE) and elemental analyses were obtained under a low vacuum mode with an accelerating voltage of 15 kV. The EDS analyses were performed under similar magnifications at the same working distance (10 mm), and with the same acquisition time (100 s) for each EDS spectrum. The mineralogical composition of modified and unmodified iron-rich lumps was determined by Raman spectroscopy using the same equipment employed on shaped beads. For these last samples, the measurements were done with a 785 nm laser and a power of 1 mW in order to avoid thermal transformation of mineral phases. The spectra were recorded with an integration time varying from 5 to 10 s, in a spectral range from 100 to 2200 cm^{-1}, and with a number of co-additions varying between 15 to 25 depending on the presence of fluorescence radiation and signal-to-noise ratio.

Results

Personal ornaments

Five main personal ornament categories were recorded at Panga ya Saidi: perforated *Conus* spires, OES beads, perforated marine gastropods, circular shell beads and tubular shell beads (Figures 3-10). We present here a description of these artifacts and provide information on their technological, morphological and dimensional variability. Results concerning these artifacts are summarised in Tables 1-2.

Perforated Conus sp. *spires*

These objects are fragments of *Conus* shells resulting from the natural degradation of the thick shells and robust spires belonging to this genus (Table 1). Destruction of these shells begins with the gradual fading of the pattern, and continues with the fracture of the outer lip, bioerosion, opening of perforations on the body whorl, progressive reduction of the latter by fracture and/or erosion until only the spire, or fragments of the remainder of the shell survive (Figure S1). Degradation proceeds with the gradual erosion of the spire, leading to the eventual opening of a hole at the apex (Claassen, 1998; d'Errico and Backwell, 2016). When occurring on *Conus* shells with flat spires the perforation may give the impression that the spire was flattened by abrasion to open a hole at the apex. *Conus* fragments at this final stage of destruction, consisting of polished dome-shaped disks with a perforation in the middle, commonly known as "puka shells", are intensively used for jewellery in Hawaii (Mattes, 1974). Similar uses are attested in Africa (Harding, 1961). The size of the perforations in puka shells increases proportionally as the fragments reduce in size. This explains why the perforations on *Conus* fragments recovered at Panga ya Saidi display, comparatively to other bead types, a wide range of variation. The distance of Panga ya Saidi from the coast and identification of two cases in which the natural perforations were marginally modified favour an interpretation of these shell fragments as beads. Apart from two specimens found in Layers 16 and 10, this bead type is concentrated in Layers 8 and 9, where 17 of the beads were recovered. The two specimens that show possible evidence of modification come from Layers 16 and 8. The first exhibits traces of grinding followed by polishing of the spire in an area close to the perforation (Figure S2, A). The second shows on the perforation edge a small well-preserved area covered with striations possibly indicating that the hole was slightly enlarged by rotation (Figure S2, B).

Ostrich egg shell beads

Eighty-eight OES beads were recovered at Panga ya Saidi. A single specimen comes from Layer 9. The large majority of the others come from Layers 7-8, only a dozen from Layers 5-6, and five from Layers 2-4. Breathing pores detected on well preserved areas of the egg outer surface are concentrated in clusters of individual pores or alignments of pores (Figure S3). This feature indicates that *Struthio camelus massaicus* and/or *Struthio camelus molybdophanes* are the more likely sub-species that have produced the eggs employed to make the beads (Schönwetter, 1927, Sauer, 1972). This attribution is consistent with the present geographical distribution of these sub-species. *S. camelus massaicus* is common in Kenya and southern Somalia, *S. camelus molybdophanes* in Ethiopia and northern Somalia. The two subspecies are sympatric in a large north-west to south-east oriented band covering the north of Kenya and the south of Somalia, which may have shifted during the Upper Pleistocene in response to climatic changes. Although variably modified by abrasion and polishing, the egg thickness measured on the beads (mean of 1.77 mm with a range between 1.32 mm and 2.16 mm) is consistent with these attributions.

Morphological and technological analyses (Figure S4) reveal notable differences in OES beads manufacture and style within and between layers. Six main types are identified (Figure 9): Type A includes large circular OES beads with large perforations. They exhibit polished to highly polished faces, elliptical and often slightly off-centred perforations, and straight or slightly convex edges in cross section. The edge formed by the intersection of the egg shell's original surface with the perforation is very regular on the inner shell surface (interior perforation edge), but very irregular on the outer surface (exterior perforation edge). This indicates that the perforation was made from the inner toward the outer surface of the egg shell (Wei et al., 2017). Type B includes very large circular OES beads with relatively small perforations. These beads exhibit slightly polished faces, circular perfectly centred perforations, and slightly convex edges in cross-section. Interior and exterior perforation edges are both slightly irregular. Type C includes small polygonal OES beas with small polygonal perforations. These beads exhibit scars left by trimming the edge of the bead preform, smoothed by polish, very convex edges in cross section, bi-conical perforations with very flared edges and very irregular interior and exterior perforation edges. Type D includes sub-circular/ovoid OES beads with circular perforations. These beads exhibit polished to highly polished surfaces, slightly irregular interior and exterior perforation edges, and variable edge shape along their cross sections. Type E includes small circular OES beads with comparatively large circular perforations, diffused interior and exterior perforation edges, and convex cross-sections all over the bead surface. Type F includes very small OES beads with very small perforations. These beads exhibit highly polished faces, circular perfectly centred perforations, perfectly straight edges in cross section, and cylindrical perforations with very regular interior and exterior perforation edges. Eight OES beads do not fall into these categories. Each of them exhibits a distinct combination of dimensional and technological features (Figure S5). One is sub-circular in shape and bears a very small perforation with flared edges (Figure 5, n. 33; Figure S5, A). A second has a general morphology reminiscent of type B while being smaller in size and displaying flared perforation edges (Figure 5, n. 35; Figure S5, B). A third is also reminiscent of type B but differs from the OES beads attributed to this type by its smaller size, irregular outline and bi-conical perforation with flared edges (Figure 5, n. 53; Figure S5, C). A fourth associates the perforation size and general appearance of type A OES beadds with a polygonal outline (Figure 5, n. 57; Figure S5, D). A fifth consists of a small OES beads with a polygonal outline, a small perforation with flared edges on the inner side of the egg, and a polish reminiscent of type A (Figure 4, n. 7; Figure S5, E). A sixth differs from the previous one in that it exhibits a circular outline and is characterised by an even more flared perforation edge on the inner side of the egg (Figure 4, n. 8; Figure S5, F). A seventh associates an irregular sub-circular outline with a small perforation and a very convex edge in cross section (Figure 3, n. 16; Figure S5, G). The eighth is larger than type F, but smaller than the other beads, and differs from the OESBs attributed to type F in the bi-conical shape of the perforation (Figure 3, n. 48; Figure S5, H).

Apart from two specimens, found in Layer 5, Type A is concentrated in Layers 7-8. Types B is also concentrated in Layers 7-8 with two specimens of this type found in Layers 6 and one, the lowermost OESB recovered at the site, in Layer 9. Six of the seven specimens of Type C are also found in Layers 7-8, the seventh coming from Layer 5. Type D and E are only present in Layers 5-6 and Type F in Layers 2 and 3.

Thirty-three OES beads (37%) bear evidence of having been heated to darken them. This treatment is, in fourteen cases, responsible for the splitting of the bead (Figure 5). Only OES beads belonging to Types A, B, and D were submitted to this treatment, which was not used for the small irregular beads of Type C and E, nor for the three small OES beads found in Layer 2 and 3. Interestingly, heating was applied to morphologically and dimensionally similar beads made of marine shells, found in the same layers (see below). Four of the eight beads falling outside the main OES bead types have also been heated (Figure S6). Differences in shade suggest that the technique was not equally mastered. Type A OESBs exhibit, when heated, a very dark black shade, which is also found in those attributed to Type D and one of the unclassified OESBs (Figures S4 and S5). This black shade is only rarely observed with Type B OESBs. Around 70% of OESBs, from all layers, bear residues of possible pigment on the perforation and faces, less frequently on the edge (Figure S7). All beads exhibit traces of utilization suggesting that they have been lost or disposed of after being used as personal ornaments (Figure S4).

Morphometric analysis of OESBs confirms to a great extent the grouping based on visual discrimination. The scatterplot correlating bead and perforation maximum diameters (Figure 10) shows that Types A and B cluster separately and are characterised by mutually exclusively bead and perforation sizes. This suggests that the grooved stones used to produce them and drilling tools that have perforated them were different. Type C beads are smaller than Type B and their perforations fall outside Type A and F variation. They represent the only type of beads having a wide range in diameter and a high degree of correlation between diameter of the hole and the bead. Due to their irregular morphology and size, as well as their poor manufacture quality, the artisan/s adapted the size of the perforation to that of the bead, possibly to reduce the risk of breakage. The three specimens attributed to Type D have diameters incompatible with types A, B, E, and F, the two ascribed to type E have diameters incompatible with Types A, B, D and F. Finally, the three beads assigned to Type F, all from Layer 6, are significantly different in size and perforation diameter from those belonging to all other types and two of them cluster with the circular marine shell bead recovered in the same layer (see below). Of the eight OES beads falling outside the type range of morphometric variability, one from Layer 7-8, displays, as with two of Type F, the same perforation size of the circular shell beads found in that layer (Figure 3, n. 48), but falls at the very end of their bead diameter variability. Similarly, another falls within the range of the perforation diameter of Type B (Figure 5, n. 57). The other six beads have sizes incompatible with Types A, B, E, and F but present a relatively large variation in perforation size.

In conclusion, the analysis of the OES beads found at Panga ya Saidi identifies discrete groups of beads, each characterised by a combination of technological, stylistic, morphological and dimensional features, plus a small group of OESBs, different from each other and from those belonging to the main types.

Differences between Types A, B, C and E are striking and consistent, in the light of OES beads variability observed ethnographically and archaeologically (d'Errico et al., 2012; Wei et al., 2017; Pitarch Marti et al., 2017), with the interpretation of each of these groups of beads as having been made by the same craftsperson or crafts people sharing the same know-how, motions, and aesthetic. It is possible some beads belonging to the same type originate from the same beadwork, partially lost or deliberately disposed of at the site. The beads not allocated to specific types likely represent objects coming from different beadworks and individually lost at the site. A possible exception is represented by the bead dimensionally clustering with Group A and sharing other features with the beads from this group (Figure 5, n. 57), but presenting an irregular outline. This bead could belong to this group in spite of its idiosyncratic shape. The fact that single specimens belonging to Types A, B and C are found in neighbouring layers may be due to mobility across layers or fuzzy limits between the cultural traditions represented in these layers and Layers 7-8. OES beads of Type F and the small bead falling, morphometrically, outside this group (Figure 3, n. 48), tell a different story. They come from layers dated to historical periods and mostly fit into the morphometric variability of relatively standardized circular beads made of marine shells (see below). This suggests that during this recent period, OES became a raw material to produce beads comparable in size to those made of marine shell.

Perforated marine gastropods

Five perforated marine gastropods (Table 3) were recovered at Panga ya Saidi: one *Volvarina* sp. in Layer 11 (Figure 8, n. 1), two others in Layer 4 (Figure 3, n. 47) and Layers 1-2 (Figure 3, n. 5), one perforated *Cypraea annulus* in Layer 3 (Figure 3, n. 28) and one *Cypraea moneta* in Layer 2 (Figure 3, n. 15). The three *Volvarina* sp. are, despite their different stratigraphic provenances, relatively comparable in size and exhibit on their dorsal aspect similar elongated perforations aligned along the shell longitudinal axis. The perforation edges have irregular, micro denticulate outlines, suggesting that the perforation was enlarged by exerting pressure with a pointed tool on the perforation edge (Figure S8). This technique was probably also employed to produce the large irregular perforation on the *C. annulus* from Layer 3. The smaller off-centred perforation on the shell from the same genus found in Layer 2 was instead opened by first creating a large facet by abrasion and subsequently opening a hole by puncturing the dwindled shell wall (Figure S9). Abrasion was also applied, on this shell, on the surface surrounding the facet on which the perforation was made and on the outer lip, which exhibits striations oriented along the shell main axis. All the perforated gastropods bear traces of utilization indicating that they were lost or disposed of after being used as personal ornaments.

Manufactured shell beads

Forty small disk or cylindrical shaped shell beads and a possible unfinished bead were recovered at Panga ya Saidi (Table 2; Figures 3-4). With the exception of two specimens, found in Layer 5, all the others come from Layers 1-4. The possible unfinished bead is one of the two from Layer 5 (Figure 4, n. 3), and it consists of a tubular undetermined fossil exhibiting a hole at one end and no compelling evidence of deliberate modification. All the other beads bear diagnostic evidence of human manufacture. Most of these beads were correctly identified as made of marine shell at the moment of discovery. A number of them, however, black to dark-brown in colour, were tentatively interpreted in the field as made of stone, possibly slate or shale. In order to determine the raw material, Raman analysis were conducted on four of these latter beads (Table 2). Results indicate in all cases that the main component is calcite (Raman bands at 155, 281, 712, 1085, 1260, 1298 and 1437 cm^{-1}), which rules out slate, and is consistent with their production from marine shell (Figure S10). Raman analysis also identifies, in two cases, the presence of amorphous carbon (bands 1351 and 1600 cm^{-1}), and in one case the presence of anatase (TiO_2, Raman bands at 147, 199, 398, 515, 638 cm^{-1}). Incorporation of amorphous carbon is the consequence of heat treatment in a reductive environment conducted with the aim of blackening the beads (d'Errico et al., 2015). This may also explain the absence of aragonite. If naturally present in the shell, this mineral, was transformed to calcite by the heating process. Incorporation of anatase could result from the use of a tool or an abrasive powder made of a titanium rich-rock to shape the bead prior to heating, or a substance incorporated during the heating process.

Although the degree of modification undergone by these beads makes it difficult in a number of cases to identify the type of shell used as a raw material and the technique of manufacture, some Panga ya Saidi beads show features providing information on these topics. Three cylindrical beads (Figure 3, n. 4, 27, 46) retain on their curved surface shallow depressions identified as the folds of marine gastropod columellas. This indicates that these beads were made, as with pre-Columbian examples from Illinois, by carefully chipping away the body whorl and spire of large marine gastropods, incising and snapping the exposed columella, and shaping the resulting tubular blank by grinding (Kozuch, 2007). These three beads show no evidence of heating, which suggests that, unlike their pre-Columbian counterparts, fire was not used to weaken the body whorl before chipping it away. Remnants of bivalve sculpture consisting of undulations or individual grooves are identified on one side of many of the other beads (Figure 3, n. 6-10, 12-13, 18-19, 29, 31- 38, 49; Figure 4, n. 2; Figure S11). This suggests that the technique used to produce these beads entailed, as with OES beads, trimming fragments of marine bivalves, grinding them on a grooved stone, polishing them and, in some cases blackening them by heating. The thickness of these beads, ranging from 0.5 to 4.1 mm, indicates that a large variety of bivalves were used to produce them. Morphometric analysis (Figure 10) reveals, compared to OES beads groups, a wide size range associated with a relatively narrow, although quite variable, perforation size interval. This pattern likely reflects episodes of loss of single or multiple beads coming from many similar beadworks, produced originally by numerous crafts people using slightly different drilling tools. The perforation size and its cylindrical morphology suggest the use of a bow-drill, although two specimens exhibit elliptical holes that may result from the use of a hand-drill.

Long term morphometric trends

In addition to the differences in OES bead technology, colour, and size mentioned above a general trend toward a reduction in bead size is observed from the bottom to the top of the sequence (Figure S12). Beads in Layers 7-8 are tightly clustered with maximum dimensions between about 7.5 and 9 mm, and Layers 5 and 6 demonstrate an overall reduction toward mean diameters of around 7 mm. If all disk beads (OES and marine shell) are considered together, a dramatic reduction in bead maximum dimension occurs with the Iron Age layers (1-4), when bead maximum dimensions plunge to around 4.5 mm.

Worked bone

Six objects made of bone and teeth bear clear evidence of deliberate modification (Table 3). Two worked suid canines, probably tusks of bushpig (*Potamochoerus larvatus*) or warthog (*Phacochoerus* *aethiopicus*) come from Layer 10 and one from Layers 7-8 (Figure 6, n. 11; Figure 7, n. 20-21). The first two are fragments of tusks, longitudinally split before being manufactured by scraping on the resulting break (Figure S13). Although the fragments are too small to establish with certainty what kind of tool was sought, the pointed outline of one fragment suggests it may have been an awl. The piece from Layers 7-8 is a fragment of a tusk tip preserving portions of the anterior, lingual and labial outer surfaces covered by enamel, the masticatory surface, and a longitudinal break (Figure S13). In adult wild suids, canine masticatory surfaces are generally covered with parallel striations, mimicking grinding, perpendicular or slightly oblique to the main axis of the canine (d'Errico et al., 2012). In this case, the remnant of the masticatory surface is covered by striations produced by scraping, parallel to the tooth long axis. In addition, this surface is obliquely crossed by a deep groove made by a stone tool, which may have been used to facilitate the longitudinal splitting of the tusk. Similar tools have been reported from Border Cave, South Africa from MSA and early LSA layers dated to between 60 ka and 44 ka (d'Errico et al., 2012). Another category of artifacts found in Layer 9 is represented by a single specimen (Figure 7, n. 14; Figure S14). This is a mesial fragment of a thin point made of a small mammal long bone, shaped by scraping. Diameter and technique of manufacture are consistent with the interpretation of this object as a fragment of an arrow point comparable to those found at a few early LSA sites in southern Africa (d'Errico et al., 2012; Backwell and d'Errico, 2016; Backwell et al., 2018, but see Bradfield, 2016), ubiquitous at later LSA sites, and still in use among historical San hunter-gatherers. Shot with small bows, these arrow points are generally covered with poison in order to be effective when hunting large mammals.

Four objects from Layer 9 and Layers 7-8 are either fragments of decorated bone tubes made of small mammal limb bones or byproducts of their manufacture (Figure 7, n. 1-2; Figure 6; n. 12-13). The two fragments from Layer 9 do not refit, but judging from their similar thickness and manganese stain pattern, may have originally been part of the same artifact. The larger fragment exhibits a set of eighteen equidistant notches. The second has a set of eleven. Microscopic analysis indicates that each set was made by a single tool, likely during a single episode (Figure S15). The lithic tool was in both cases a straight unretouched cutting edge, as indicated by the narrow, asymmetrical section of the notches and absence of steps on their angled side (d'Errico, 1998). The two objects from Layers 7-8 are a bone tube decorated on one side with two sets of notches and the epiphyseal fragment of a long bone bearing a groove obliquely cutting the diaphysis. The latter is likely the leftover of an unsuccessful attempt to produce a bone tube by first cutting a deep perpendicular notch around the diaphysis and then snapping it by flexion (Figure 6, n. 12). The former is a fragmentary bone tube bearing evidence at the preserved end of having being produced with the same technique (Figure 6, n. 13). The sets of notches cut on this object were originally composed by at least eight and eleven notches each. Both sets were likely made by the same tool during a single episode (this interpretation is made on the basis of a photograph, as this object was unfortunately lost by the courier during export).

Fossil

Layer 9 yielded a mesio-distal fragment of the rostrum of a belemnite exhibiting at its ends an old and a recent fracture (Figure 7, n. 13). The longitudinally-oriented groove, corresponding to the remnant of the siphon located on the back side of the rostrum, presents no trace of modification. The object is highly polished and traces of abrasion are detected close to the ancient break (Figure S16). Although no comparative material was available to characterize the natural appearance of rostra from geographically close paleontological outcrops, the unusual polish suggests that the object was curated, and possibly used as a tool or an ornament. The missing, naturally pointed end may have been used for piercing. Rostra were used as personal ornaments in the Upper Paleolithic of Europe (Vanhaeren and d'Errico, 2006; Sinitsyn, 2010). San people use similar objects, carved out of pebbles, with a slightly wider groove, as arrow straighteners. The San peoples place them in hot sand before placing the arrow shaft in the groove and gently bend it.

Ochre pieces

Seventeen lumps of ochre, yellow to dark red in colour, were identified as mineral pigments and analyzed (Table 4). They come from Layers 7, 8, 10, and 16-18. Only two of them, from Layers 8 and 10, bear clear traces of modification (Figure 6, n. 14; Figure 7, n. 19). We provide below a description, technological analysis and physicochemical characterization of these two last objects before presenting results concerning the unmodified pieces. A summary of the results is given in Tables S1-S3.

Modified iron-rich pieces

One piece of ochre from Layer 8 is a large fragment of an originally fully shaped iron-rich flat nodule (Figure 6, n. 14; Figure S17). The largest triangular surfaces, corresponding to the nodule's original flat sides, show evidence of having being shaped by pecking and polishing. The combination of these two techniques produced a rough surface with pits and incipient fractures alternating with flat polished areas that are covered by randomly oriented microscopic striations. Located between these two surfaces, a flat area exhibiting two adjacent aligned facets is covered by subparallel striations oriented along the nodule longest axis. They result from vigorous abrasion of this area against a lower grindstone in a direction parallel to the nodule edge. The fracture that split the object served as a platform to remove two small adjacent flakes that create a denticulated edge, as well as a point. The latter bears microscopic evidence that it was used to mark a surface with thin red streaks. In summary, this lump bears evidence of having been purposely shaped, used as a source of raw material to produce a relatively coarse pigment powder, and split and retouched to be used as a crayon. The shaping and multiple modifications and use suggest that the object was curated. The fracture reveals a thick layer of fine-grain matrix crossed by randomly-oriented cleavages surrounding an amorphous core. Under optical microscopy, the outer layer is composed of spots of dark red alternating with spots of red fine-grained matrix. No visible grains are scattered within the matrix.

EDXRF elemental analysis identifies iron (Fe), calcium (Ca), manganese (Mn), and strontium (Sr) and, at a trace level, phosphor (P), potassium (K), titanium (Ti), zinc (Zn), and yttrium (Y) (Figure S18). SEM-EDS analysis indicates that the sample is composed of iron-oxide particles (Fe) associated with silicates (Si) and aluminosilicates (Si, Al, K) (Figure S19). Most aluminosilicates take the form of sub-micrometric particles (clay fraction). Micrometric particles are also identified, suggesting the presence of micas and/or feldspars. Other elements detected by SEM-EDS include Mg, P, Ca, Ti and Mn. Raman analysis identifies hematite (Fe_2O_3, Raman bands at 222, 291, 403, 486, 605, and 1286 cm^{-1}), calcite ($CaCO_3$, main Raman band 1085 cm^{-1}), and quartz (SiO_2, main Raman band at 459 cm^{-1}) (Table S2, Figure S20). Intense fluorescence background and bands in the region between 1120 and 1415 cm^{-1} suggest the presence of clay minerals. In some cases, a few weak bands appear in the region of 500–700 cm^{-1}, characteristic of Mn–O and Mn–OH bending and stretching vibrations. In addition, gypsum – possibly a by-product of a weathering process - ($CaSO_4$ $2H_2O$, Raman bands at 414, 493, 669, 1007 and 1027 cm^{-1}) – is also identified on the specimen surface.

A fragment from Layer 10, trapezoidal in shape, displays an angled edge along its longitudinal axis. It exhibits on its convex aspect a set of wide joining grooves oriented along the main axis of the object (Figure S21). Microscopic analysis indicates that the grooves were engraved by the same tool, in a single episode, and that the craftsman deliberately terminated some lines or changed their direction to create a recognizable pattern. This indicates that the lines were not made with the intent to produce pigment powder. A few thin, parallel lines, oriented along the long axis of the object, are engraved on the concave aspect of the piece. Two small opposing flake scars are located on one corner of its narrower end.

Under optical microscopy, the fragment is composed of a dark red to orange compact homogeneous clay with no grains scattered in the matrix. EDXRF elemental analysis identifies Fe, Ca, and Mn, together with P, K, Ti, and Sr (Figure S22). SEM-EDS analysis indicates that the piece is composed of iron-oxide particles (Fe) associated with silicates (Si), and aluminosilicates (Si, Al, K) (Table S3, Figure S23). Silicates take the form of 5 µm wide or smaller rounded particles (Figure 28D-

E; Figure 29A). Most aluminosilicates consist of sub-micrometric particles (clay fraction), or, less frequently, rounded micrometric tablets of micas and/or feldspars (see Figure S23 D and E, spectrum SP1). Iron-oxides take the shape of sorted and rounded 2.5 µm wide particles (Figure S23 D-E, spectrum SP2). Other elements present in the object matrix include carbon (C), magnesium (Mg), P, sulphur (S), Ca, Ti, and Mn. The spatial distribution of the detected elements (Figure S24) shows that Al is mostly associated with Si, but also with Fe. Ca is associated with P, and Mg. Mn is homogeneously distributed and associated with Fe. In addition, the mapping identifies particles mostly composed of C and S (Figure S23 D-E-SP3 and Figure S24) possibly biological in origin. Raman analysis finds hematite, calcite and quartz as well as bands between 1120 and 1415 cm^{-1}, characteristic of clay minerals (Table S2, Figure S25).

The finer-grained texture of the piece from Layer 10 compared to that from Layer 8, the lower content in Ti and Mn, the presence of C, and the absence of Y indicate that these two objects may come from different sources.

Unmodified iron-rich rock lumps

Fifteen other fragments collected during the excavation as possible lumps of red ochre are all significantly smaller that the two modified pieces, more friable, and present a coarser granulometry (Figure 6, n. 9-10; Figure 7, n. 23-25; Figure 8, n. 2, 4-7; 9-12). They show a range in variation that extends from ferruginous lutite to ferruginous fine and very fine sandstone. Colour, texture, grain size, and mineral content suggest that nine different sedimentary rock types are represented (Tables S1 and S2). Hematite is identified by µ-RS in half of these lumps (Table S2). A number, particularly those orange to dark red in shade, have clear colouring power. Some of these fragments may derive from crushing larger lumps to produce pigment powder. This hypothesis would be reinforced by the demonstration that these materials, or at least some of them, do not occur naturally in the site sediment.

Discussion and conclusion

The analysis of several categories of key artifacts recovered from Panga ya Saidi opens up new opportunities to explore how the material culture of populations living in the coastal areas of eastern Africa integrated, since 78 ka, innovations reflecting the emergence of behaviorally ‘modern’ cultures.

The inferences that can be drawn from this material are limited by the fact that certain types of objects, present in large numbers in a number of layers, were discovered in older layers exclusively in the form of a single specimen or specimens that do not show diagnostic traces of modification. It may therefore be premature to take their earliest occurrence in the stratigraphy as definite evidence that the behaviours associated with these objects are contemporary with the layer in which they first appear. The iron oxide rich fragments from Layers 18-16 may indicate that red pigment was brought and perhaps processed at the site between 76 ka and 67 ka, but to be able to affirm this with certainty in the absence of traces of modification on these objects, it would have to be demonstrated that this material is not naturally present at the site, which requires dedicated work in the field and additional analyses.

While the bulk of the Panga ya Saidi assemblage does not represent ‘earliest’ occurrences of osseous tools and symbolic artifacts, it does provide a unique record for deep-time behavioural patterns leading to intensification of important phenomena like bead production. Furthermore, the high-resolution palaeoecological record for the site and the emerging datasets on stone tools and other materials offer great potential to understand the context for the emergence of symbolic traits. If these circumstances can be reconstructed from the Panga ya Saidi dataset, it may offer new analogical structures for investigating “earliest” occurrences and testing hypotheses relating changes in symbolic styles with changes in population structures. The Panga ya Saidi assemblage itself adds an important data point to an emerging picture of diverse symbolic trajectories through the MSA and LSA of eastern Africa.

The first definite evidence of an interest in ochre use appears in Layer 10 (between 48.5-33 ka, for Layers 11-9). Such interest is manifested by the use of an ochre fragment as a media for engraving rather than for intense extraction of colour powder, the latter of which is only demonstrated by an object in Layer 8 (ca. 25 ka). A similar caveat applies to the only puka shell found in Layer 16 (bracketed by dates of 67 ka – 61.5 ka) and the perforated *Volvarina* sp. discovered in Layer 11 (48.5 ka). The first layers in which several puka shells appear in association are Layers 9 (33 ky) and 8 (25 ka), and the other two *Volvarina* sp. shells discovered so far come from Layer 4 (7.5 ky) and Layers 1-2 (ca. 1 ka), and have a perforation very similar to the specimen from Layer 11. This raises the question as to whether puka shells are an ornament that emerged in this region in the late MSA (67-61.5 ka) or whether their appearance is contemporary with the first OES beads, around 33 ka. In the former scenario, it would be the first indication that marine shell beads preceded OES beads in eastern Africa in a pattern more comparable to that seen in southern Africa. If the latter is supported by future evidence, the sudden investment in forms of exo-somatic symbolism may reflect major changes in demographic dynamics at this time. What is clear is that these puka shells were certainly used as ornaments between 33 ka and 25 ka, and that they are absent in Layer 6 (>25 ka) in which OES beads are found. Additionally, Panga ya Saidi is the first site in which they are found in Africa, making them an icon of the cultural trajectory of the coastal populations of the region.

Almost all typical OES beads come from Layers 5-8 (25-14 ka). The single specimens from Layer 9 (33 ka) and Layers 2-4 may indicate sporadic loss of this ornament type contemporaneous with the deposition of those layers or post-depositional displacement. The second hypothesis is reinforced for the more recent specimens by the presence, in those layers, of numerous tiny circular beads, some of which are made of OES, so that the two larger OES beads found in those layers are idiosyncratic occurrences. The alternative hypothesis is that during the deposition of recent layers the site was alternatively occupied by users of both bead types or that the occupants of the cave used both bead types. If the stratigraphic distribution of bead types is confirmed by the analysis of the material from the more recent excavation seasons at Panga ya Saidi and at other sites, this may indicate that OES beads were first in use in some coastal regions of East Africa later than in inland areas, the earliest occurrences of this bead type being dated in Kenya, Tanzania and South Africa between 50 ka and 31 ka (Miller and Willoughby 2014; see Wei et al., 2017 for a synthesis).

The absence of ostrich remains, egg shell fragments, bead preforms, the intense use-wear recorded on all OES beads and the numerous specimens bearing ochre residues suggest that the beads were lost or disposed of, but not manufactured at the site, at least in the spatial locality investigated by our trench. The current distribution of the two ostrich species that probably provided the eggs from which the beads discovered at Panga ya Saidi were produced is limited to grassland plateaus, the closest of which occur today about 100 kilometres west of the site (Sinclair, 2003). It is unlikely, in light of climate model outputs for the LGM (Shipton et al., 2018), that grasslands have spread, even in drier periods, to coastal areas. This is consistent with our results and, together with the fact that Panga ya Saidi is the only site in eastern Africa with a bead assemblage that lacks any indication of early stage working or preforms, suggests that OES beads should be considered exotic items at Panga ya Saidi. Clear differences in OES beads technology, size, style, and heat-induced colouring indicate that different human groups carrying different variants of these ornaments visited the site during the deposition of Layers 5-8; that one group had access to the traditions of different groups through exchange; or that one resident group employed two different traditions of OES bead manufacture.

The OES beads from Panga ya Saidi also demonstrate a trend toward smaller diameters through the sequence, similar to the size reduction noted for the Pleistocene layers at Kisese II (Tryon et al., 2017). This dramatic discontinuity in bead material and size may be the best evidence for changes in population structure. It is interesting to note in this respect that an individual burial from the site dating to 400 BP retains strong East African forager ancestry (Skoglund et al., 2017).

However the bead manufacture and size patterns are interpreted, they appear to be unique for eastern Africa and may reflect the coast experiences different cultural influences, developments or population histories relative to inland areas. Hypotheses that needs to be explored in this regard are that puka shells may reflect the identity of coastal populations before the spread of OES beads into these areas, and that the site has been occupied or visited during at least some periods by different populations, some wearing puka shells and others OES beads, or that the people frequenting the site were wearing both. Whatever the case, a clear shift in bead technology and types occurs at the beginning of the Holocene, when small circular beads made of marine shells and OES, perforated cowrie and *Volvarina* shells, and small tubular beads made of the columellas of large marine gastropods replace large OES beads. An important caveat is that many older excavations in the Central Rift Valley employed 5mm screen sizes, and so some bead size distributions may have be biased.

The only other Pleistocene African site that has yielded worked suid tusks is Border Cave (d'Errico et al., 2012), where they were processed with techniques similar to those identified at Panga ya Saidi and mostly occur in layers roughly contemporaneous with those in which they are found at Panga ya Saidi. At Border Cave, however, a few pieces come from older, 60 ka layers, while the artifact from Panga ya Saidi comes from Layer 7-8 (25 ka). At Border Cave, as at other early LSA sites from Southern Africa (Backwell et al., 2012; Backwell and d'Errico 2016), we find the two other bone artifact categories identified at Panga ya Saidi: bone diaphyses carrying sets of notches, and thin bone artifacts interpreted as pins or possible arrow points used with poison (d'Errico et al., 2012; Backwell et al., 2018). The peculiarity of the Panga ya Saidi objects belonging to the first category lies in the fact that two of them bear clear traces of having been cut with the groove-and-snap technique to produce bone tubes that may have been used as containers, and that the set of notches have been apparently made by a single tool and in an attempt to juxtapose them equidistantly, which points to a decorative rather than notational function (d'Errico et al., 2018). Although the bone rod found in Layer 9 is broken, making it difficult to attribute this object to an artifact category, its diameter falls in the variability of LSA and historical bipointed arrowheads from southern Africa (d'Errico et al., 2012; Robbins et al., 2012).

Bone implements and especially the notched piece artifact in Pleistocene contexts are typologically and temporally similar to those reported for Kuumbi Cave on the Tanzanian coast (Langley et al., 2016). Taken together, the Panga ya Saidi and Kuumbi Cave datasets indicate a tradition of bone tool production and use by c. 20,000 BP on the coast of eastern Africa that predates any comparable pattern inland by nearly 10,000 years. The early appearance of worked bone traditions on the coast relative to inland is an interesting contrast to the apparently opposite pattern discussed above for OES beads.

When evaluated in a pan-African context Panga ya Saidi records the emergence, perhaps as early as 67 ka or at 33 ka, of an original symbolic material culture (puka shells) replaced, possibly later than elsewhere, by symbolic items (ostrich egg shell beads) and bone artifacts (worked suid tusks, small bone point, notched bone containers) showing similarities with those identified at sites in southern Africa located in subtropical areas, such as at Border Cave and Sibudu. The identified trend is consistent with a more fragmented cultural geography until ca. 40 ka, followed by the adoption of cultural innovations that may have emerged in neighbouring regions and arrived by cultural diffusion to East Africa. OES beads, in particular, suggest the creation of exchange networks with inland areas. These are replaced, at the beginning of the Holocene, by a more varied body ornamentation primarily exploiting marine resources that includes bead types whose production required a degree of craft specialisation.

It is therefore clear that the processes initiated by the first appearances of symbolic behaviours in the MSA are not part of a single event, but rather cascading shifts toward in regional connections and diversifications over many millennia. Further investigation is needed to understand the degree to which this may reflect growing biological or ethnic boundaries among Pleistocene foragers.

In summary, Panga ya Saidi is important as it is, at present, the only site located outside north-west and southern Africa, the two classic regions in which key cultural innovations have been identified in MSA contexts, to deliver, in a well dated sequence, a record of cultural innovations of diverse types over a time span covering the late MSA and the LSA. Together, the results highlighted here are consistent with a scenario in which both regional trajectories and cultural/demic diffusion acted, at different times, as the driving factors shaping cultural diversity in Africa. Ongoing analyses of material from recent excavation campaigns at Panga ya Saidi and other sites will allow testing of the patterns identified here, and further document the emergence and long-term evolution of personal ornaments, bone technologies, and ochre use in eastern Africa.

Acknowledgements

This research was supported by grants from the European Research Council (FP7/2007/2013, TRACSYMBOLS 249587 and SEALINKS 206148), the *Agence Nationale de la Recherche* – LaScArBx Cluster of Excellence (ANR-10-LABX-52) project "CUMILA: Cultural Innovations in the Middle and Later Stone Age of East Africa: Panga ya Saïdi, Kenya", the Research Council of Norway through its Centre of Excellence funding scheme (SFF Centre for Early Sapiens Behaviour –SapienC– project number 262618), and the Max Planck Society. Permission to conduct research was granted by the Office of the President of the Republic of Kenya through affiliation with the National Museums of Kenya. We are grateful for the support and assistance of these institutions as well as the British Institute in Eastern Africa. Research by APM was funded by the LabEx and the Beatriu de Pinós postdoctoral programme of the Government of Catalonia's Secretariat for Universities and Research of the Ministry of Economy and Knowledge (2017 BP-A 00046). FD, APM and EL are grateful to Mourer-Chauviré for providing references and advice on the identification of ostrich egg sub-species and to Isabelle Svahn (Bordeaux Imaging Center) for her assistance with the SEM-EDS analysis. We thank the Panga ya Saidi field teams, including local peoples, especially Jackson Mupe, Yahya Lenga, Emmanuel Mupe, and Mohammed Lenga, and student volunteers, John Mpangarusiya, Tim McEnright, and Doreen Mutoro.

References

Ackermann, R. R., Mackay, A., Arnold, M.L., 2016. The Hybrid Origin of Modern Humans. Evolutionary Biology 43 (1), 1–11.

Adler, D. S., Wilkinson, K. N., Blockley, S., Mark, D. F., Pinhasi, R., Schmidt-Magee, B. A., Nahapetyan, S., Mallol C., Berna, F., Glauberman, P.J., Raczynski-Henk, Y., Wales, N., Frahm, E., Jöris, O., MacLeod, A., Smith, V.C., Cullen, V.L., Gasparian, B., 2014. Early Levallois technology and the Lower to Middle Paleolithic transition in the Southern Caucasus. Science 345 (6204), 1609-1613.

Aranguren, B., Revedin, A., Amico, N., Cavulli, F., Giachi, G., Grimaldi, S., Macchioni, N., Santaniello, F., 2018. Wooden tools and fire technology in the early Neanderthal site of Poggetti Vecchi (Italy). Proceedings of the National Academy of Sciences 115 (9), 2054-2059.

Ashton, N., Scott, B., 2016. The British Middle Palaeolithic. Quaternary international, 411, 62-76.

Assefa, Z., Asrat, A., Hovers, E., Lam, Y., Pearson, O., & Pleurdeau, D., 2018. Engraved ostrich eggshell from the Middle Stone Age contexts of Goda Buticha, Ethiopia. Journal of Archaeological Science: Reports 17, 723-729.

Backwell, L.R., d’Errico, F., 2001. Termite gathering by Swartkrans early hominids. Proceedings of the National Academy of Sciences 98 (4), 1358–1363.

Backwell, L., d’Errico, F., 2005. The origin of bone tool technology and the identification of early hominid cultural traditions. In: d’Errico, F., Backwell, L. (Eds.), From Tools to Symbols: From Early Hominids to Modern Humans. Witwatersrand University Press, Johannesburg, pp. 238-275.

Backwell, L.R., d'Errico, F., Banks, W.E., de la Peña, P., Sievers, C., Stratford, D., Lennox, S.J., Wojcieszak, M., Bordy, E.M., Bradfield, J., Wadley, L., 2018. New Excavations at Border Cave, KwaZulu-Natal, South Africa. Journal of Field Archaeology 43 (6), 417-436.

Backwell, L., d'Errico, F., Wadley, L., 2008. Middle Stone Age bone tools from the Howiesons Poort layers, Sibudu Cave, South Africa. Journal of Archaeological Science 35 (6), 1566-1580.

Barham, L., 2002. Systematic pigment use in the Middle Pleistocene of south-central Africa. Current anthropology 43 (1), 181-190.

Bicho, N., Cascalheira, J., André, L., Haws, J., Gomes, A., Gonçalves, C., Raja, M., Benedetti, M., 2018. Portable art and personal ornaments from Txina-Txina: a new Later Stone Age site in the Limpopo River Valley, southern Mozambique. Antiquity, 92 (363).

Binford, L. R., 2014. Bones: ancient men and modern myths. Studies in Archaelogy. Academic Press, New York

Blinkhorn J., Achyuthan H., Petraglia M. D. (2014) Ostrich expansion into India during the Late Pleistocene : Implication for continental dispersal corridors, Paleogeography, Paleoclimatology, Paleoecology, 417, pp. 80-90.

Bonnichsen, R., Sorg, M.H. (Eds.), 1989. Bone modification. Center for the Study of the First Americans, Institute for Quaternary Studies, University of Maine, Orono, Maine.

Bousman, C. B., Brink, J. S., 2018. The emergence, spread, and termination of the Early Later Stone Age event in South Africa and southern Namibia. Quaternary international 495, 116-135.

Bouzouggar, A., Barton, N., Vanhaeren, M., d'Errico, F., Collcutt, S., Higham, T., Hodge, E., Parfitt, S., Rhodes, E., Schwenninger, J.-L., Stringer, C., Turner, E., Ward, S., Moutmir, Stambouli A., 2007. 82,000-year-old shell beads from North Africa and implications for the origins of modern human behavior. Proceedings of the National Academy of Sciences 104 (24), 9964-9969.

Bouzouggar, A., Humphrey, L.T., Barton, N., Parfitt, S.A., Balzan, L.C., Schwenninger, J.L., El Hajraoui, M.A., Nespoulet, R., Bello, S.M., 2018. 90,000 year-old specialised bone technology in the Aterian Middle Stone Age of North Africa. PLoS ONE 13 (10), e0202021.

Brandt, S., Hildebrand, E., Vogelsang, R., Wolfhagen, J., Wang, H., 2017. A new MIS 3 radiocarbon chronology for Mochena Borago Rockshelter, SW Ethiopia: Implications for the interpretation of Late Pleistocene chronostratigraphy and human behavior. Journal of Archaeological Science: Reports 11, 352-369.

Brooks, A.S., Helgren, D.M., Cramer, J.S., Franklin, A., Hornyak, W., Keating, J.M., Klein, R.G., Rink, W.J., Schwarcz, H., Smith, J.N.L., Stewart, K., Todd, N.E., Verniers, J., Yellen, J.E., 1995. Dating and context of three Middle Stone Age sites with bone points in the Upper Semliki Valley, Zaire. Science 268 (5210), 548-553.

Brooks, A.S., Yellen, J.E., Potts, R., Behrensmeyer, A.K., Deino, A.L., Leslie, D.E., Ambrose, S.H., Ferguson, J.R., d’Errico, F., Zipkin, A.M., Whittaker, S., Post, J., Veatch, E.G., Foecke, K., Clark, J.B., 2018. Long-distance stone transport and pigment use in the earliest Middle Stone Age. Science 360 (6384), 90-94.

Browning, S.R., Browning, B.L., Zhou, Y., Tucci, S., & Akey, J.M., 2018. Analysis of human sequence data reveals two pulses of archaic denisovan admixture. Cell 173 (1), 53-61.

Bruner, E., 2014. Functional craniology, human evolution, and anatomical constraints in the Neanderthal braincase. In: Akazawa, T., Ogihara, N., Tanabe, H.C., Terashima, H. (Eds.), Dynamics of learning in Neanderthals and modern humans Volume 2, Cognitive and Physical Perspectives Springer Japan, Tokyo, pp. 121–129.

Burrough, S.L., Thomas, D.S.G., & Barham, L.S., 2019. Implications of a new chronology for the interpretation of the Middle and Later Stone Age of the upper Zambezi Valley. Journal of Archaeological Science: Reports 23, 376-389.

Chikhi, L., Rodríguez, W., Grusea, S., Santos, P., Boitard, S., Mazet, O., 2018. The IICR (inverse instantaneous coalescence rate) as a summary of genomic diversity: insights into demographic inference and model choice. Heredity 120 (1), 13-24.

Choyke, A., Bartosiewicz, L., 2001. Crafting Bone: Skeletal Technologies Through Time and Space, Proceedings of the 2nd meeting of the (ICAZ) Worked Bone Research Group Budapest, 31 August 5 September 1999, BAR International Series 937, Oxford.

Claassen, C., 1998. Shells. Cambridge University Press, Cambridge.

Coolidge, F.L., Wynn, T., 2017. The rise of Homo sapiens: The evolution of modern thinking. *Oxford University Press*, Oxford, UK.

d'Errico, F., 1995. A new model and its implications for the origin of writing: the La Marche antler revisited. Cambridge Archaeological Journal 5 (02), 163-206.

d’Errico, F., 1998. Palaeolithic Origins of Artificial Memory Systems: an Evolutionary Perspective. In: Renfrew, C., Scarre, C. (Eds.), Cognition and Material Culture: the Archaeology of Symbolic Storage. McDonald Institute Monographs, Cambridge, pp. 19–50.

d’Errico, F., Backwell, L., 2016. Earliest evidence of personal ornaments associated with burial: the *Conus* shells from Border Cave. Journal of Human Evolution 93, 91-108.

d'Errico, F., Nowell, A., 2000. A new look at the Berekhat Ram figurine: implications for the origins of symbolism. Cambridge Archaeological Journal 10 (01), 123-167.

d’Errico, F., Giacobini, G., Puech, P.-F., 1984. An experimental study on the technology of boneimplement manufacturing. MASCA J 3 (3), 71–74.

d'Errico, F., Jardon, P., Soler, B., 1993. Etude des perforations naturelles et artificielles sur coquillages. In: Anderson, P.C., Beyries, S., Otte, M., Plisson H. (Eds.), Traces et Fonction: les gestes retrouvés. Actes du Colloque international de Liège, 8-9-10 décembre 1990. ERAUL Etudes et recherches archéologiques de l'université de Liège. Série A 50, pp. 243–254.

d'Errico, F., Henshilwood, C., Vanhaeren, M., Van Niekerk, K., 2005. *Nassarius kraussianus* shell beads from Blombos Cave: evidence for symbolic behaviour in the Middle Stone Age. Journal of Human Evolution 48 (1), 3-24.

d'Errico, F., Vanhaeren, M., Barton, N., Bouzouggar, A., Mienis, H., Richter, D., Hublin, J.-J., McPherron, S.P., Lozouet, P., 2009. Additional evidence on the use of personal ornaments in the Middle Paleolithic of North Africa. Proceedings of the National Academy of Sciences 106 (38), 16051-16056.

d'Errico, F., Backwell, L., Villa, P., Degano, I., Lucejko, J.J., Bamford, M.K., Higham, T.F.G., Colombini, M.P., Beaumont, P.B., 2012. Early evidence of San material culture represented by organic artifacts from Border Cave, South Africa. Proceedings of the National Academy of Sciences 109 (33), 13214-13219.

d'Errico, F., Moreno, R.G., Rifkin, R.F., 2012. Technological, elemental and colorimetric analysis of an engraved ochre fragment from the Middle Stone Age levels of Klasies River Cave 1, South Africa. Journal of Archaeological Science 39 (4), 942-952.

d'Errico, F., Vanhaeren, M., Van Niekerk, K., Henshilwood, C.S., Erasmus, R.M., 2015. Assessing the Accidental Versus Deliberate Colour Modification of Shell Beads: a Case Study on Perforated *Nassarius kraussianus* from Blombos Cave Middle Stone Age levels. Archaeometry 57 (1), pp. 51–76.

d'Errico, F., Banks, W.E., Warren, D.L., Sgubin, G., van Niekerk, K., Henshilwood, C., Daniau, A.-L., Goñi, M. F. S., 2017. Identifying early modern human ecological niche expansions and associated cultural dynamics in the South African Middle Stone Age. Proceedings of the National Academy of Sciences 114 (30), 7869-7876.

d'Errico, F., Doyon, L., Colagé, I., Queffelec, A., Le Vraux, E., Giacobini, G., Vandermeersch, B., Maureille, B., 2018. From number sense to number symbols. An archaeological perspective. Philosophical Transactions of the Royal Society B: Biological Sciences, 373 (1740), 20160518.

De la Peña, P., Val, A., Stratford, D.J., Colino, F., Esteban, I., Fitchett, J.M., Hodgskiss, T., Matembo, J., Moll, R., 2018. Revisiting Mwulu's Cave: new insights into the Middle Stone Age in the southern African savanna biome. Archaeological and Anthropological Sciences 1-28.

Dediu, D., Levinson, S.C., 2018. Neanderthal language revisited: not only us. Current opinion in behavioral sciences 21, 49-55.

Dirks, P.H.G.M., Berger, L.R., Hawks, J., Randolph-Quinney, P.S., Backwell, L.R., & Roberts, E.M., 2016. Deliberate body disposal by hominins in the Dinaledi Chamber, Cradle of Humankind, South Africa?. Journal of Human Evolution 30, 1e5.

Dirks, P.H., Roberts, E.M., Hilbert-Wolf, H., Kramers, J.D., Hawks, J., Dosseto, A., Duval, M., Elliott, M. vans, M., Grün, R., Hellstrom, J., Herries, A.I.R., Joannes-Boyau, R., Makhubela, T.V., Placzek, C. J., Robbins, J., Spandler, C., Wiersma, J., Woodhead, J., Berger, L.R., 2017. The age of Homo naledi and associated sediments in the Rising Star Cave, South Africa. eLIFE, 6, e24231.

Doerschner, N., Fitzsimmons, K.E., Ditchfield, P., McLaren, S.J., Steele, T.E., Zielhofer, C., McPherron, S.P., Bouzouggar, A., Hublin, J.J., 2016. A new chronology for Rhafas, northeast Morocco, spanning the North African Middle Stone Age through to the Neolithic. PLoS ONE, 11 (9), e0162280.

Durvasula, A., Sankararaman, S., 2018. Recovering signals of ghost archaic admixture in the genomes of present-day Africans. *bioRxiv*, 285734.

Fogarty, L., Wakano, J.Y., Feldman, M.W., Aoki, K., 2017. The driving forces of cultural complexity. Human Nature 28 (1), 39-52.

Fu, Q., Hajdinjak, M., Moldovan, O.T., Constantin, S., Mallick, S., Skoglund, P., Patterson, N., Rohland, N., Lazaridis, I., Nickel, B., Viola, B., Prüfer, K., Meyer, M., Kelso, J., Reich D., Pääbo, S., 2015. An early modern human from Romania with a recent Neanderthal ancestor. Nature 524 (7564), 216.

Giaccio, B., Hajdas, I., Isaia, R., Deino, A., & Nomade, S., 2017. High-precision 14 C and 40 Ar/39 Ar dating of the Campanian Ignimbrite (Y-5) reconciles the time-scales of climatic-cultural processes at 40 ka. Scientific Reports 7, 45940.

Harding, J.R., 1961. *Conus* shell disc ornaments (Vibangwa) in Africa. Journal of the Royal Anthropological Institute of Great Britain and Ireland 91(1), 52–66.

Harris, K., Nielsen, R., 2016. The genetic cost of Neanderthal introgression. Genetics, 203 (2), 881-891.

Hawks, J., Elliott, M., Schmid, P., Churchill, S.E., de Ruiter, D.J., Roberts, E.M., Hilbert-Wolf H., Garvin, H.M., Williams, S.A., Delezene, L.K., Feuerriegel, E.M., Randolph-Quinney, P., Kivell, T.L., Laird, M.F., Tawane, G., DeSilva, J.M., Bailey, S.E., Brophy, J.K., Meyer, M.R., Skinner, M.M., Tocheri, M.W., VanSickle, C., Walker, C.S., Campbell, T.L., Kuhn, B., Kruger, A., Tucker, S., Gurtov, A., Hlophe, N., Hunter, R., Morris, H., Peixotto, B., Ramalepa, M., Rooyen, D.V., Tsikoane, M., Boshoff, P., Dirks, P.H., Berger, LR., 2017. New Fossil Remains of Homo Naledi from the Lesedi Chamber, South Africa. eLIFE 1–63.

Henn, B.M., Gignoux, C.R., Jobin, M., Granka, J.M., Macpherson, J.M., Kidd, J. M., Rodríguez-Botigué, L., Ramachandran, S., Hon, L., Brisbin, A., Lin, A.A., Underhill, P.A., Comas, D., Kidd, K.K., Norman, P.J., Parham, P., Bustamante, C.D., Mountain, J.L., Feldman, M.W., 2011. Hunter-gatherer genomic diversity suggests a southern African origin for modern humans. Proceedings of the National Academy of Sciences 108 (13), 5154-5162.

Henn, B.M., Steele, T.E., & Weaver, T.D., 2018. Clarifying distinct models of modern human origins in Africa. Current opinion in genetics & development 53, 148-156.

Henshilwood, C.S., d'Errico, F., Yates, R., Jacobs, Z., Tribolo, C., Duller, G.A., Mercier, N., Sealy, J.C., Valladas, H., Watts, I., Wintle, A.G., 2002. Emergence of modern human behavior: Middle Stone Age engravings from South Africa. Science 295 (5558), 1278-1280.

Henshilwood, C.S., d'Errico, F., Watts, I., 2009. Engraved ochres from the Middle Stone Age levels at Blombos Cave, South Africa. Journal of Human Evolution 57 (1), 27-47.

Henshilwood, C.S., Dubreuil, B., 2011. The Still Bay and Howiesons Poort, 77–59 Ka. Current Anthropology 52 (3) 361–400.

Henshilwood, C.S., van Niekerk, K.L., Wurz, S., Delagnes, A., Armitage, S.J., Rifkin, R.F., Douze, K., Keene, P., Haaland, M.M., Reynard, J., Discamps, E., Mienies, S.S., 2014. Klipdrift shelter, southern Cape, South Africa: preliminary report on the Howiesons Poort layers. Journal of Archaeological Science 45, 284-303.

Hodgskiss, T., 2010. Identifying grinding, scoring and rubbing use-wear on experimental ochre pieces. Journal of Archaeological Science 37, 3344-3358.

Hoffmann, D.L., Standish, C.D., García-Diez, M., Pettitt, P.B., Milton, J.A., Zilhão, J., Alcolea-González, J.J., Cantalejo-Duarte, P., Collado, H., de Balbín, R., Lorblanchet, M., Ramos-Muñoz, J., Weniger, G.-Ch., Pike, A.W.G., 2018. U-Th dating of carbonate crusts reveals Neandertal origin of Iberian cave art. Science 359 (6378), 912-915.

Hu, Y., Marwick, B., Zhang, J. F., Rui, X., Hou, Y. M., Yue, J. P., Chen, W.-R., Huang, W.-W., Li, B., 2019. Late Middle Pleistocene Levallois stone-tool technology in southwest China. Nature 565 (7737), 82.

Hublin, J.J., Ben-Ncer, A., Bailey, S.E., Freidline, S.E., Neubauer, S., Skinner, M.M., Bergmann, I., Le Cabec, A., Benazzi, S., Harvati, K., Gunz, P., 2017. New fossils from Jebel Irhoud, Morocco and the pan-African origin of Homo sapiens. Nature, 546 (7657), 289.

Jacobs, Z., Roberts, R.G., 2015. An improved single grain OSL chronology for the sedimentary deposits from Diepkloof Rockshelter, Western Cape, South Africa. Journal of Archaeological Science 63, 175-192.

Jacobs, Z., Meyer, M.C., Roberts, R.G., Aldeias, V., Dibble, H., El Hajraoui, M.A., 2011. Single-grain OSL dating at La Grotte des Contrebandiers (‘Smugglers’ Cave’), Morocco: improved age constraints for the Middle Paleolithic levels. Journal of Archaeological Science 38 (12), 3631-3643.

Jacobs, Z., Roberts, R.G., Galbraith, R.F., Deacon, H. J., Grün, R., Mackay, A., Mitchell, P., Vogelsang, R., Wadley, L., 2008. Ages for the Middle Stone Age of southern Africa: implications for human behavior and dispersal. Science 322 (5902), 733-735.

Jacobs, Z., Roberts, R.G., Nespoulet, R., El Hajraoui, M.A., Debénath, A., 2012. Single-grain OSL chronologies for Middle Palaeolithic deposits at El Mnasra and El Harhoura 2, Morocco: Implications for Late Pleistocene human–environment interactions along the Atlantic coast of northwest Africa. Journal of Human Evolution 62 (3), 377-394.

Jaubert, J., Verheyden, S., Genty, D., Soulier, M., Cheng, H., Blamart, D., Burlet, C., Camus, H., Delaby, S., Deldicque, D., Edwards, R.L., Ferrier, C., Lacrampe-Cuyaubère, F., Lévêque, F., Maksud, F., Mora, P., Muth, X., Régnier, É., Rouzaud, J.-N., Santos, F., 2016. Early Neanderthal constructions deep in Bruniquel Cave in southwestern France. Nature 534 (7605), 111.

Johansson, S., 2015. Language abilities in Neanderthals. Annual Review of Linguistics 1 (1), 311-332.

Joordens, J.C., d'Errico, F., Wesselingh, F.P., Munro, S., De Vos, J., Wallinga, J., Ankjærgaard, C., Reimann, T., Wijbrans, J.R., Kuiper, K.F., Mücher, H. J., Coqueugniot, H., Prié, V., Joosten, I., van Os, B., Schulp, A.S., Panuel, M., van der Haas, V., Lustenhouwer, W., Reijmer, J.J.G. Roebroeks, W., 2015. Homo erectus at Trinil on Java used shells for tool production and engraving. Nature 518 (7538), 228.

Kandel, A., Conard, N., 2005. Production sequences of ostrich eggshell beads and settlement dynamics in the Geelbek Dunes of the Western Cape, South Africa. Journal of Archaeological Science 32, 1711– 1721.

Klein, R.G., 2007. Anatomy, behavior, and modern human origins. Journal of World Prehistory 9.2, 167-198.

Kozuch, L., 2007. Replication of Busycon Columella Shell Beads, Illinois Archaeology, 15-16: 142–157.

Lafuente, B., Downs, R.T., Yang, H., Stone N., 2015. The power of databases: the RRUFF project. In: Armbruster, T., Danisi, R.M. (Eds.), Highlights in Mineralogical Crystallography, Berlin, Germany, W. De Gruyter, pp. 1-30.

Locht, J.L., Hérisson, D., Goval, E., Cliquet, D., Huet, B., Coutard, S., Antoine, P., Feray, P., 2016. Timescales, space and culture during the Middle Palaeolithic in northwestern France. Quaternary International 411, 129-148.

Loftus, E., Mitchell, P.J., Ramsey, C.B., 2019. An archaeological radiocarbon database for southern Africa. Antiquity https://doi.org/10.17863/CAM.35023

Loftus, E., Sealy, J., Lee-Thorp, J., 2016. New radiocarbon dates and Bayesian models for Nelson Bay Cave and Byneskranskop 1: Implications for the South African Later Stone Age sequence. Radiocarbon 58 (2), 365-381.

Mackay, A., Welz, A., 2008. Engraved ochre from a Middle Stone Age context at Klein Kliphuis in the Western Cape of South Africa. Journal of Archaeological Science 35 (6), 1521-1532.

Majkić, A., Evans, S., Stepanchuk, V., Tsvelykh, A., d'Errico, F., 2017. A decorated raven bone from the Zaskalnaya VI (Kolosovskaya) Neanderthal site, Crimea. PLoS ONE 12 (3), e0173435.

Martí, A.P., Wei, Y., Gao, X., Chen, F., & d'Errico, F., 2017. The earliest evidence of coloured ornaments in China: The ochred ostrich eggshell beads from Shuidonggou Locality 2. Journal of Anthropological Archaeology 48, 102-113.

Mattes, P.J., 1974. Puka shell Hawaii: The story of puka shell jewelry in the Hawaiian Islands. Hawaiian Puka Shell, Hawaii.

Mayer, D. E.B.Y., Vandermeersch, B., Bar-Yosef, O., 2009. Shells and ochre in Middle Paleolithic Qafzeh Cave, Israel: indications for modern behavior. Journal of Human Evolution 56 (3), 307-314.

Mourer-Chauviré C., Geraads D., 2008. The Struthionidae and Pelagornithidae (Aves: Sthruthioniformes, Odontopterygiformes) from the Late Pliocènes of Ahl Al Oughlam, Morocco, Oryctos 7, pp. 169-194

Neubauer, S., Hublin, J.J., Gunz, P., 2018. The evolution of modern human brain shape. Science advances 4 (1), eaao5961.

Newcomer, M.H. (1974). Study and replication of bone tools from Ksar Akil (Lebanon). World Archaeology 6 (2), 138-153.

Orton, J., 2008. Later Stone Age ostrich eggshell bead manufacture in the Northern Cape, South Africa. Journal of Archaeological Science 35, 1765–1775.

Pagani, L., Kivisild, T., Tarekegn, A., Ekong, R., Plaster, C., Gallego Romero, I., Ayub, Q., Mehdi, S.Q., Thomas, M.G., Luiselli, D., Bekele, E., Bradman, N., Balding, D.J., Tyler-Smith, C., 2012. Ethiopian genetic diversity reveals linguistic stratification and complex influences on the Ethiopian gene pool. The American journal of Human genetics 91 (1), 83-96.

Patin, E., Quintana-Murci, L., 2018. The demographic and adaptive history of central African hunter-gatherers and farmers. Current opinion in genetics & development 53, 90-97.

Pettitt, P., 2010. The Palaeolithic origins of human burial. Routledge, London.

Pleurdeau, D., 2005. Human technical behavior in the African middle stone age: the lithic assemblage of Porc-Epic cave (Dire Dawa, Ethiopia). African Archaeological Review 22 (4), 177-197.

Porraz, G., Val, A., Tribolo, C., Mercier, N., De La Peña, P., Haaland, M.M., Igreja, M., Miller, C.E., Schmid, V.C., 2018. The MIS5 Pietersburg at ‘28’ Bushman Rock Shelter, Limpopo Province, South Africa. PLoS ONE 13 (10), e0202853.

Relethford, D.J.H., Harpending, H.C., 1994. Craniometric variation, genetic theory, and modern human origins. American Journal of Physical Anthropology 95 (3), 249-270.

Rifkin, R., 2012. Processing ochre in the Middle Stone Age: Testing the inference of prehistoric behaviours from actualistically derived experimental data. Journal of Anthropological Archaeology 31 (2), pp. 174-195

Rifkin, R.F., Henshilwood, C.S., Haaland, M.M., 2015. Pleistocene figurative art mobilier from Apollo 11 Cave, Karas Region, southern Namibia. The South African Archaeological Bulletin 70 (201), 113-123.

Rito, T., Vieira, D., Silva, M., Conde-Sousa, E., Pereira, L., Mellars, P., Richards, M.B., Soares, P., 2019. A dispersal of Homo sapiens from southern to eastern Africa immediately preceded the out-of-Africa migration. Scientific reports 9 (1), 4728.

Robbins, L.H., Campbell, A.C., Brook, G.A., Murphy, M.L., Hitchcock, R.K., 2012. The antiquity of the bow and arrow in the Kalahari Desert: bone points from White Paintings Rock Shelter, Botswana. Journal of African Archaeology 10 (1), 7-20.

Roebroeks, W., Villa, P., Trinkaus, E., 2011. On the Earliest Evidence for Habitual Use of Fire in Europe. Proceedings of the National Academy of Sciences of the United States of America108 (13): 5209–5214. doi:10.1073/pnas.1018116108.

Rosso, D.E., d'Errico, F., Zilhão, J., 2014. Stratigraphic and spatial distribution of ochre and ochre processing tools at Porc-Epic Cave, Dire Dawa, Ethiopia. Quaternary international 343, 85-99.

Rosso, D.E., d’Errico, F., Queffelec, A., 2017. Patterns of change and continuity in ochre use during the late Middle Stone Age of the Horn of Africa: The Porc-Epic Cave record. PLoS ONE 12 (5), e0177298.

Rosso, D.E., Martí, A.P., d’Errico, F., 2016. Middle Stone Age Ochre Processing and Behavioural Complexity in the Horn of Africa: Evidence from Porc-Epic Cave, Dire Dawa, Ethiopia. PLoS ONE, 11 (11), e0164793.

Sauer, E.G.F., 1972. Ratite Eggshells and Phylogenetic Questions. Bonner zoololgische Beiträge 23 (1), 3-45.

Scerri, E.M., 2017. The North African Middle Stone Age and its place in recent human evolution. Evolutionary Anthropology: Issues, News, and Reviews 26 (3), 119-135.

Scerri, E.M., Blinkhorn, J., Niang, K., Bateman, M.D., Groucutt, H.S., 2017. Persistence of Middle Stone Age technology to the Pleistocene/Holocene transition supports a complex hominin evolutionary scenario in West Africa. Journal of Archaeological Science: Reports 11, 639-646.

Schlebusch, C.M., Malmström, H., Günther, T., Sjödin, P., Coutinho, A., Edlund, H., Munters A. R., Vicente, M., Steyn, M., Soodyall, H., Lombard, M., Jakobsson, M., 2017. Southern African Ancient Genomes Estimate Modern Human Divergence to 350,000 to 260,000 Years Ago. Science 358 (6363), 652-655.

Schönwetter, M., 1927. Die Eier von Struthio camelus spatzi Stresemann. Ornithologische Monatsberichte, pp. 13-17.

Shea, J., 2011. *Homo sapiens* is as *Homo sapiens* was: Behavioral variability versus "Behavioral Modernity" in paleolithic archaeology. Current Anthropology 52 *(1)*, 1–35.

Shipman, P., Rose, J., 1988. Bone tools: an experimental approach. In: Olsen, S. (Ed.), Scanning Electron Microscopy in Archaeology. BAR International Series 452, Oxford, pp 303–335.

Shipton, C., Roberts, P., Archer, W., Armitage, S.J., Bita, C., Blinkhorn, J., Courtney-Mustaphi, C., Crowther, A., Curtis, R., d' Errico, Douka, F., K., Faulkner, P., Groucutt, H. S., Helm, R., Herries, A.I.R., Jembe, S., Kourampas, N., Lee-Thorp, J., Marchant, R., Mercader, J., Pitarch Marti, A., Prendergast, M.E., Rowson, B., Tengeza, A., Tibesasa, R., White, T.S., Petraglia, M.D., Boivin, N., 2018. 78,000-year-old record of Middle and Later stone age innovation in an East African tropical forest. Nature Communications 9, 1832.

Sinclair, I., Ryan, P., 2003. Birds of Africa south of the Sahara: A comprehensive illustrated field guide, Struik Publishers.

Sinitsyn, A.A., 2010. Figurative and decorative art of Kostenki. Chronological and Cultural Differentiation. In: Clottes, J. (Ed.), Pleistocene Art of the World. Proceedings of the IFRAO Congress pp. 1339-1359.

Slon, V., Mafessoni, F., Vernot, B., de Filippo, C., Grote, S., Viola, B., Hajdinjak, M., Peyrégne, S., Nagel, S., Brown, S., Douka, K., Higham, T., Kozlikin, M.B., Shunkov, M.V., Derevianko, A.P., Kelso, J., Meyer, M., Prüfer, K., Pääbo, S., 2018. The genome of the offspring of a Neanderthal mother and a Denisovan father. Nature 561 (7721), 113.

Soressi, M., d'Errico, F., 2007. Pigments, gravures, parures: les comportements symboliques controversés des Néandertaliens. Les Néandertaliens. Biologie et cultures, 297-309.

Steele, T.E., Álvarez-Fernández, E., Hallett-Desguez, E.: 2019. Personal Ornaments in Early Prehistory A Review of Shells as Personal Ornamentation during the African Middle Stone Age. PaleoAnthropology 24, 51.

Storz, J.F., Beaumont, M.A., 2002. Testing for genetic evidence of population expansion and contraction: an empirical analysis of microsatellite DNA variation using a hierarchical Bayesian model. Evolution 56 (1), 154-166.

Stringer, C.B., Andrews, P., 1988. Genetic and fossil evidence for the origin of modern humans. Science 239 (4845), 1263-1268.

Stringer, C., 2002. Modern human origins: progress and prospects. Philosophical Transactions of the Royal Society of London. Series B: Biological Sciences 357 (1420), 563-579.

Texier, P.J., Porraz, G., Parkington, J., Rigaud, J.P., Poggenpoel, C., Tribolo, C., 2013. The context, form and significance of the MSA engraved ostrich eggshell collection from Diepkloof Rock Shelter, Western Cape, South Africa. Journal of Archaeological Science 40 (9), 3412-3431.

Tryon, C.A., Lewis, J.E., Ranhorn, K.L., Kwekason, A., Alex, B., Laird, M.F., Marean, C.W., Niespolo, E., Nivens, J., Mabulla, A.Z., 2018. Middle and Later Stone Age chronology of Kisese II rockshelter (UNESCO World Heritage Kondoa Rock-Art Sites), Tanzania. PLoS ONE 13 (2), e0192029.

Val, A., 2016. Deliberate body disposal by hominins in the Dinaledi Chamber, Cradle of Humankind, South Africa. Journal of Human Evolution 96, 145-148.

Vanhaeren, M., d'Errico, F., 2006. Aurignacian ethno-linguistic geography of Europe revealed by personal ornaments. Journal of Archaeological Science 33, 1105–1128.

Vanhaeren, M., Wadley, L., d'Errico, F., *in press*. Variability in Middle Stone Age symbolic traditions: the marine shell beads from Sibudu Cave, South Africa. Journal of Archaeological Science: Reports.

Villa, P., d'Errico, F., 2001. Bone and ivory points in the Lower and Middle Palaeolithic of Europe. Journal of Human Evolution 41, 69–112.

Villanea, F. A., Schraiber, J.G., 2019. Multiple episodes of interbreeding between Neanderthal and modern humans. Nature ecology & evolution 3 (1), 39.

Wakeley, J., 1999. Nonequilibrium migration in human history. Genetics 153 (4), 1863-1871.

Watts, I., 2010. The pigments from pinnacle point cave 13B, Western Cape, South Africa. Journal of Human Evolution 59 (3-4), 392-411.

Wei, Y., d'Errico, F., Vanhaeren, M., Peng, F., Chen, F., & Gao, X., 2017. A technological and morphological study of Late Paleolithic ostrich eggshell beads from Shuidonggou, North China. Journal of Archaeological Science 85, 83-104.

Wendt, W.E., 1976. 'Art Mobilier'from the Apollo 11 Cave, South West Africa: Africa's Oldest Dated Works of Art. The South African Archaeological Bulletin, 5-11.

White, T.D., Asfaw, B., DeGusta, D., Gilbert, H., Richards, G.D., Suwa, G., Howell, F.C., 2003. Pleistocene Homo sapiens from middle awash, Ethiopia. Nature 423 (6941), 742.

Will, M., Conard, N.J., Tryon, C.A., 2019. Timing and trajectory of cultural evolution on the African continent 200,000-30,000 years ago? In: Sahle, Y., Reyes-Centeno, H. Bentz, C. (Eds.), Modern Human Origins and Dispersal. Kerns Verlag, Tübingen, pp. 25-72.

Wolf, A.B., Akey, J.M., 2018. Outstanding questions in the study of archaic hominin admixture. PLoS genetics, 14 (5), e1007349.

Wurz, S., 2019. Human Evolution, Archaeology and the South African Stone Age Landscape During the Last 100,000. The Geography of South Africa: Contemporary Changes and New Directions, 125-132.

Yellen, J.E., 1998. Barbed bone points: tradition and continuity in Saharan and sub-Saharan Africa. African Archaeological Review 15 (3), 173-198.

Yellen, J.E., Brooks, A.S., Cornelissen, E., Mehlman, M.J., Stewart, K., 1995. A middle stone age worked bone industry from Katanda, Upper Semliki Valley, Zaire. Science 268 (5210), 553-556.

Zilhão, J., Anesin, D., Aubry, T., Badal, E., Cabanes, D., Kehl, M., Klasen, N., Lucena, A., Martín-Lerma, I., Martínez, S., Matias, H., Susini, D., Steier, P., Wild, E.M., Angelucci, D.E., Villaverde, V., Zapata, J., 2017. Precise dating of the Middle-to-Upper Paleolithic transition in Murcia (Spain) supports late Neandertal persistence in Iberia. Heliyon 3 (11), e00435.

Figure captions

Figure 1. Location of Panga ya Saidi with the orography of the region and sea level at -125 m along the modern shoreline.

Figure 2. Panga ya Saidi sections indicating limits between layers and units, selected features, and the sequence chronology.

Figure 3. Personal ornaments from Layers 1-4. Scale = 1 cm.

Figure 4. Personal ornaments from Layers 5-6. Scale = 1 cm.

Figure 5. Ostrich egg shell beads from Layers 7-8. Scale = 1 cm.

Figure 6. Personal ornaments (n. 1-8), possible lumps of pigment (n. 9-10), worked tusk fragments (n.11), worked bones (n. 12-13), and heavily modified ochre lump (n. 14), all from Layers 7-8. Scale = 1 cm.

Figure 7. Worked bones (n. 1-2, 14), worked suid tusks (n. 20-21), personal ornaments (n. 3-12, 15-18), rostrum of belemnite (n. 13), engraved lump of ochre (n. 19), possible ornament (n. 22) and ochre lumps (n. 23-25) from Layer 9. Scale = 1 cm.

Figure 8. Perforated *Volvarina* sp. from Layer 11 (n.1), possible lump of ochre and *Conus* shell fragment from Layer 16 (n.2-3), possible lumps of ochre from Layers 17 and 18 (n.4-12). Scale = 1 cm.

Figure 9. Examples of OESBs identified as belonging to different types. Type A, B and C: OESBs from Layer 7-8 (context 412); Type D: OESBs from Layer 5 (context 104, spit F) (left) and Layer 6 (context 104, spit G) (right); Type E: OESBs from Layer 5, (context 104, spit F) (left) and Layer 6 (context 104 spit G) (right); Type F: OESBs from Layer 2 (context 406) (left) and Layer 3 (context 408, spit A) (right). Scale = 1 mm.

Figure 10. Scatterplot correlating maximum bead and perforation diameters of circular marine shell beads and OESB. OESB different from each other and from main types are indicated in blue.

Horizontal bands highlight differences in perforation size between marine shell beads, and OESB types A and B.

Supplementary materials

Figures

Figure S1. Top: Spiral fragments of *Conus* shells from Layer 9 (context 413, spit B (left) and spit C (center and right)). Bottom: comparable fragments from thanatocoenoses obtained from Southern African shores. Scale = 1mm.

Figure S2. A: *Conus* shell from Layer 16 (context 420); Center: 3D reconstruction of the perforation (left), and an area close to the perforation showing horizontal grooves produced by coarse abrasion partially obliterated by vertical striations resulting from polish (right). B: *Conus* shell from Layers 7-8 (context 104, spit H), with possible traces left by a tool used to enlarge the natural perforation. Scale = 1 mm.

Figure S3. Close up-view of the ostrich egg shell outer face on OESB from Layers 7-8 (context 412). Variability in pore arrangements suggests the use of eggs of *Struthio camelus massaicus* (left) and *Struthio camelus molybdophanes* (right) (Schönwetter, 1927; Sauer, 1972). Scale = 1 mm.

Figure S4. A and B: OESB from Layer 5 (context 104, spit F) (A), and Layer 3 (context 408, spit A); B: with traces of abrasion; C: OESB from Layer 2 (context 102, spit B), showing polishing of the mammillary layer; D: OESB from Layer 7-8 (context 412), preserving traces of rotation on the perforation edge. Scale = 1 mm.

Figure S5. Examples of OESBs not falling in any of the six main OESB types. A, B, C and D are from Layer 7-8 (context 412); E and F are from Layer 5 (context 104, spit F); G is from Layer 2 (context 102, spit B); H is from Layer 4 (context 408, spit B). Scale = 1 mm.

Figure S6. OESB from Layer 7-8 (context 412) showing removal of a large portion of the outer egg shell surface due to heating. Scale = 1 mm.

Figure S7. OESB from Layer 7-8 (context 412) exhibiting a thick red residue on the surface of the perforation. Scale = 1 mm.

Figure S8. *Volvarina* sp. shell from Layer 4 (context 408, spit A), showing an elongated perforation enlarged by pressure. Scale = 1 mm.

Figure S9. Top: *Cypraea moneta* from Layer 2 (context 407); bottom left and center: facet produced by grinding the body whorl surface in different direction before punching it in the middle; bottom right: subparallel striations produced by abrading the inner lip along the shell long axis. Scale = 1 mm.

Figure S10. µ-RS spectra on black beads from Layer 3 (context 408, spit C). A, see Figure 1, n. 39; B, see Figure 1, n. 40.

Figure S11. A-B: marine shell beads from Layers 1-2 (context 402) (A), and Layer 3 (context 408, spit A) bearing cylindrical perforations and striations produced by flattening the bead surface. C: marine shell bead from Layer 3 (context 408, spit A), with an off-centre ovoidal perforation. B and C show remnant of bivalve sculpture. Scale = 1 mm.

Figure S12. Stratigraphic variation in beads maximum diameter.

Figure S13. Top and centre: fragments of warthog or bushpig tusks from Layer 10 (context 414, spit D) showing scraping marks; bottom: fragment from Layer 7-8 (context 412) showing scraping marks and a deep groove. Scale = 1 mm.

Figure S14. Mesial fragment of a bone point from Layer 9 (context 413, spit C), showing longitudinal scraping (close-up view at the right). Scale = 1 mm.

Figure S15. Notched bone fragments from Layer 9 (context 413, spit A). Scale = 1 mm.

Figure S16. Mesial fragment of a belemnite rostrum from Layer 9 (context 413, spit C), showing traces of abrasion (close-up on the right)). Scale = 1 mm.

Figure S17. Iron-rich nodule from Layer 8 (context 104, spit H) presenting a variety of modification traces (see text).

Figure S18. Result of the EDXRF analysis of the Iron-rich nodule from Layer 8 (context 104, spit H) within the specimen from Layer 10, context 313, spit P. A: Location of the analyses. B: EDXRF spectrum. C: Detailed view of the spectrum.

Figure S19. SEM-EDS analysis on the specimen from Layer 8 (context 104, spit H). A-B: Location of the analysis. C: Detailed view of B in BSE mode. D: Detailed view of C.

Figure S20. µ-RS analyses on the specimen from Layer 8 (context 104, spit H). A-B: Location of the analyses. C-E: Raman spectra of different sub-areas.

Figure S21. Engraved fragment of ochre from Layer 10 (context 313, spit P).

Figure S22. Result of the EDXRF analysis of the engraved fragment of ochre from Llayer 10 (context 313, spit P) within the specimen from Layer 10 (context 313, spit P). A: Location of the analyses. B: EDXRF spectrum. C: Detailed view of the spectrum.

Figure S23. SEM-EDS analysis on the engraved fragment of ochre from Layer 10 (context 313, spit P). A: Location of the analyses. B-C: SE and BSE mode images at a low magnification. D: Detailed view in BSE mode with the location of the analyzed spots. E: EDS spectra.

Figure S24. SEM-EDS analysis of the engraved fragment of ochre from Layer 10 (context 313, spit P). Distribution of the main elements composing the analyzed area.

Figure S25. µ-RS analyses on the specimen from Layer 10 (context 313, spit P). A-B: Location of the analyses. C-D: Raman spectra of different compounds.

Tables

Table S1. Contextual data and results concerning the pigment analyses.

Table S2. Results of µ-RS analyses on iron-rich lumps from Panga ya Saidi.

Table S3. Results of semi-quantitative SEM-EDS analysis of modified ochre lump PYS-Phase4-Layer10-Context 313P

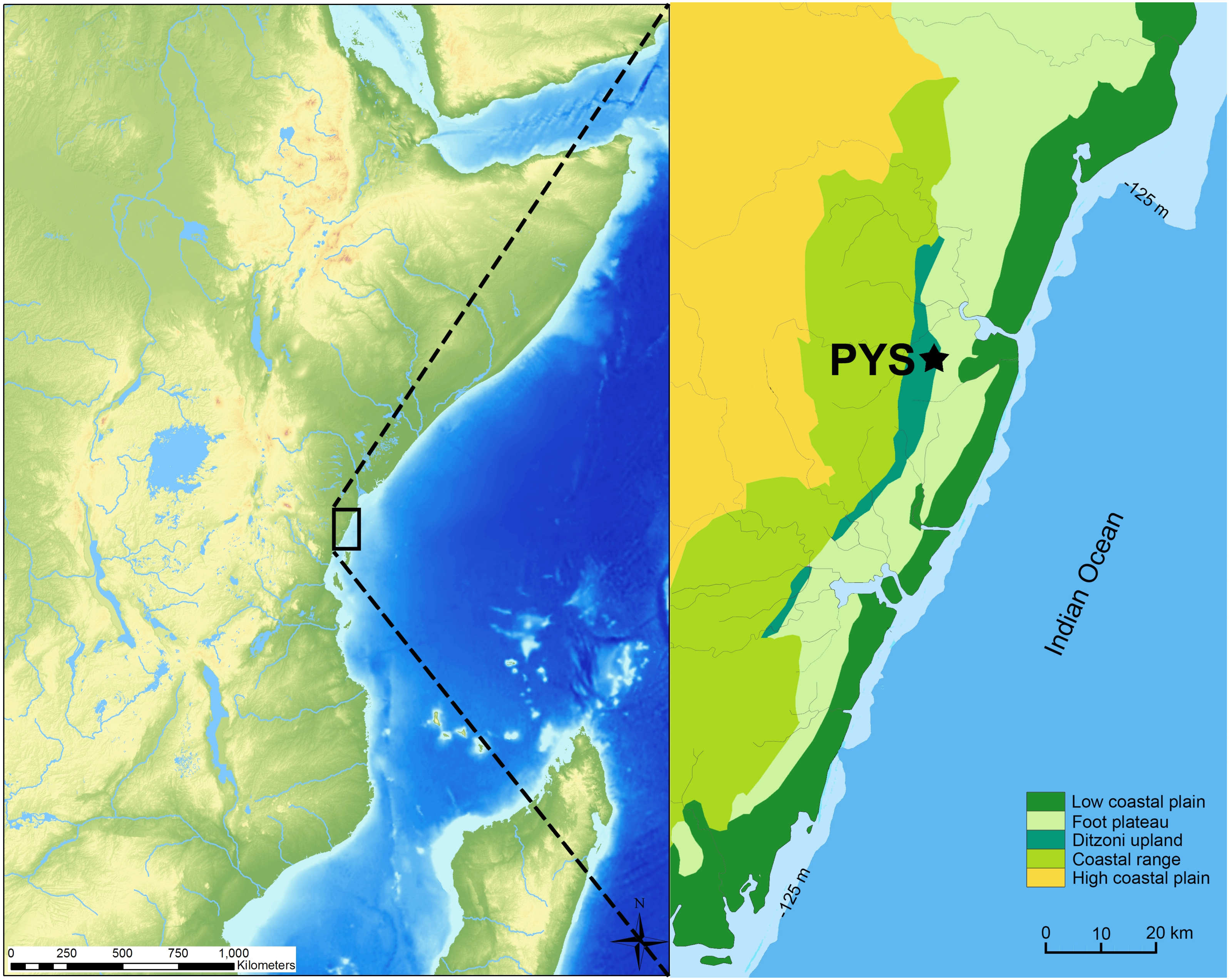
PYS
-125 m
-125 m
Indian Ocean
Low coastal plain
Foot plateau
Ditzoni upland
Coastal range
High coastal plain
0 10 20 km
0 250 500 750 1,000
Kilometers
N

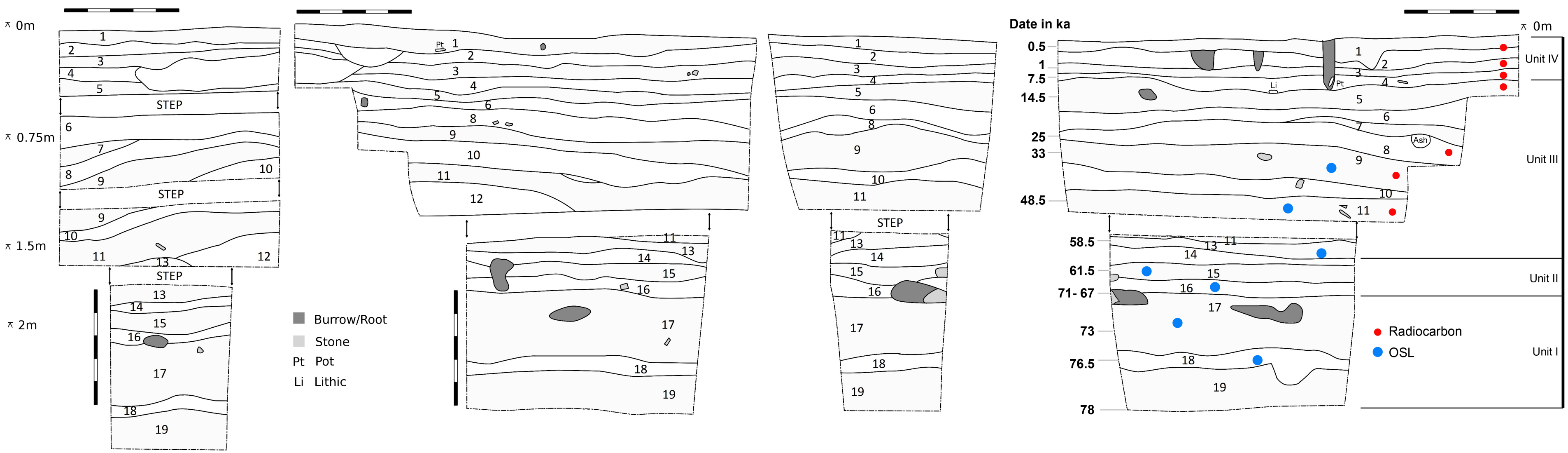

0m
0.75m
1.5m
2m
STEP
Burrow/Root
Stone
Pt Pot
Li Lithic
Date in ka
0.5
1
7.5
14.5
25
33
48.5
58.5
61.5
71- 67
73
76.5
78
Unit IV
Unit III
Unit II
Unit I
Radiocarbon
OSL
Ash


Layer 1
1
2
3
Layer 1-2
4
5
6
7
8
9
10
11
12
13
14
Layer 2
15
16
17
18
19
20
21
22
23
24
25
26
Layer 3
27
28
29
30
31
32
33
34
35
36
37
38
39
40
41
42
43
44
45
Layer 4
46
47
48
49
50
51

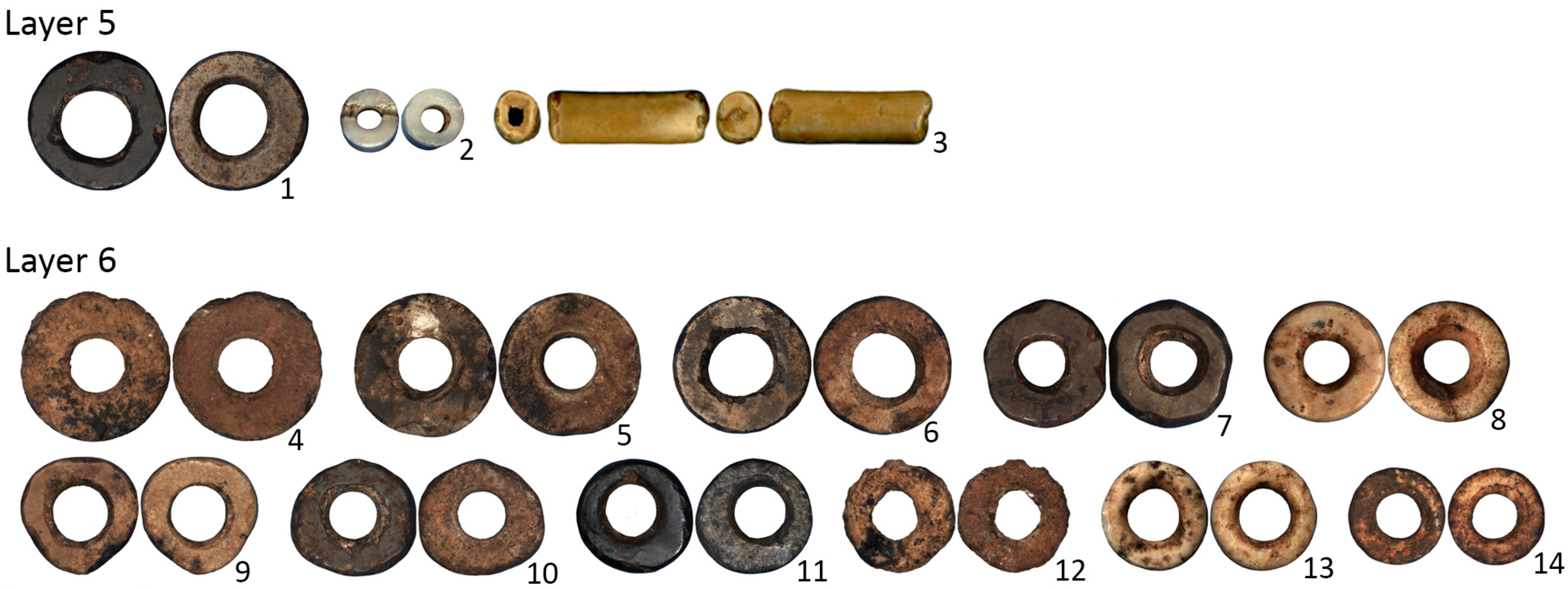
Layer 5
1
2
3
Layer 6
4
5
6
7
8
9
10
11
12
13
14

Layer 7-8

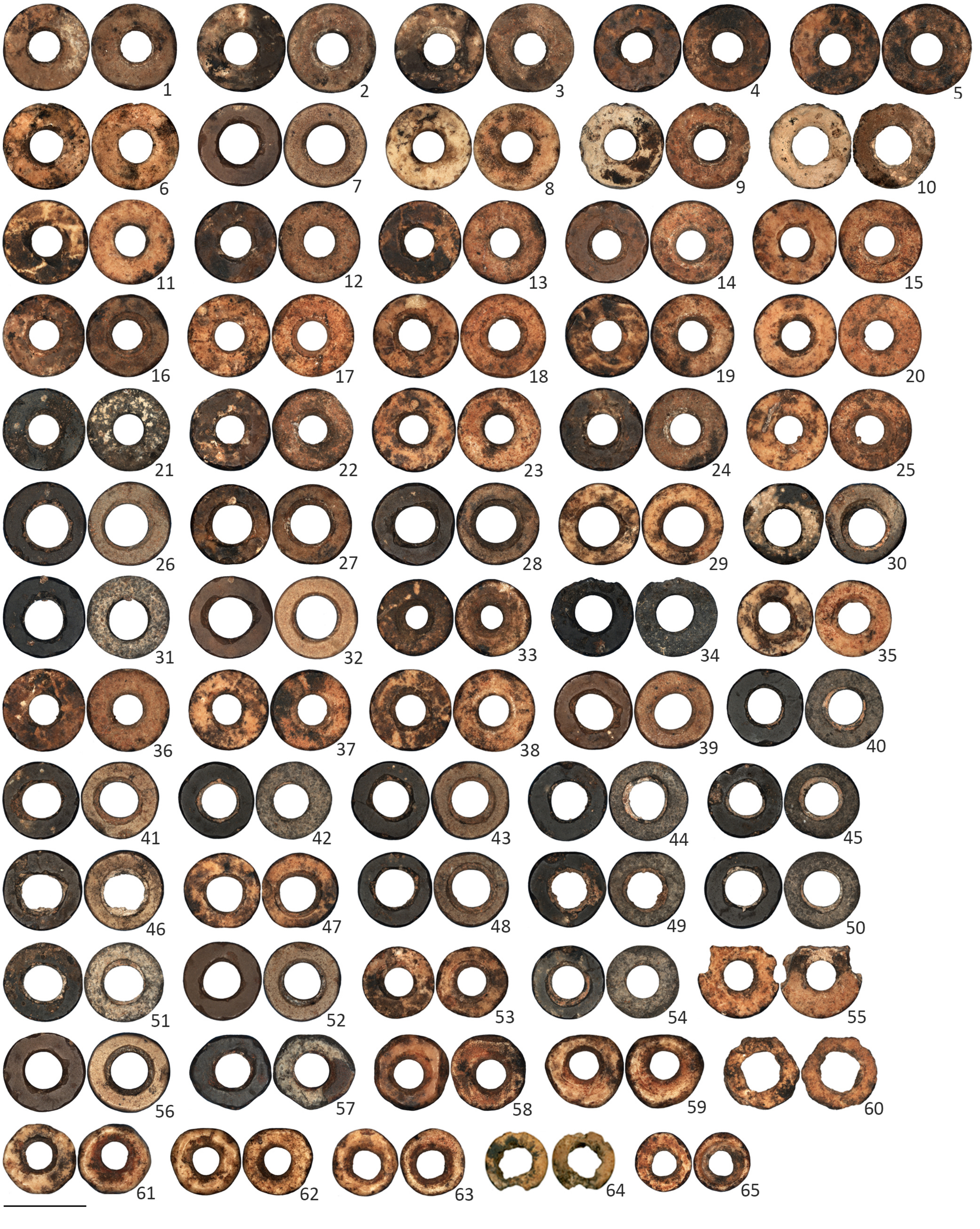

Layer 7-8

Layer 9
1
2
3
4
5
6
7
8
9
10
11
12
13
14
15
16
17
18
Layer 10
19
20
21
22
23
24
25

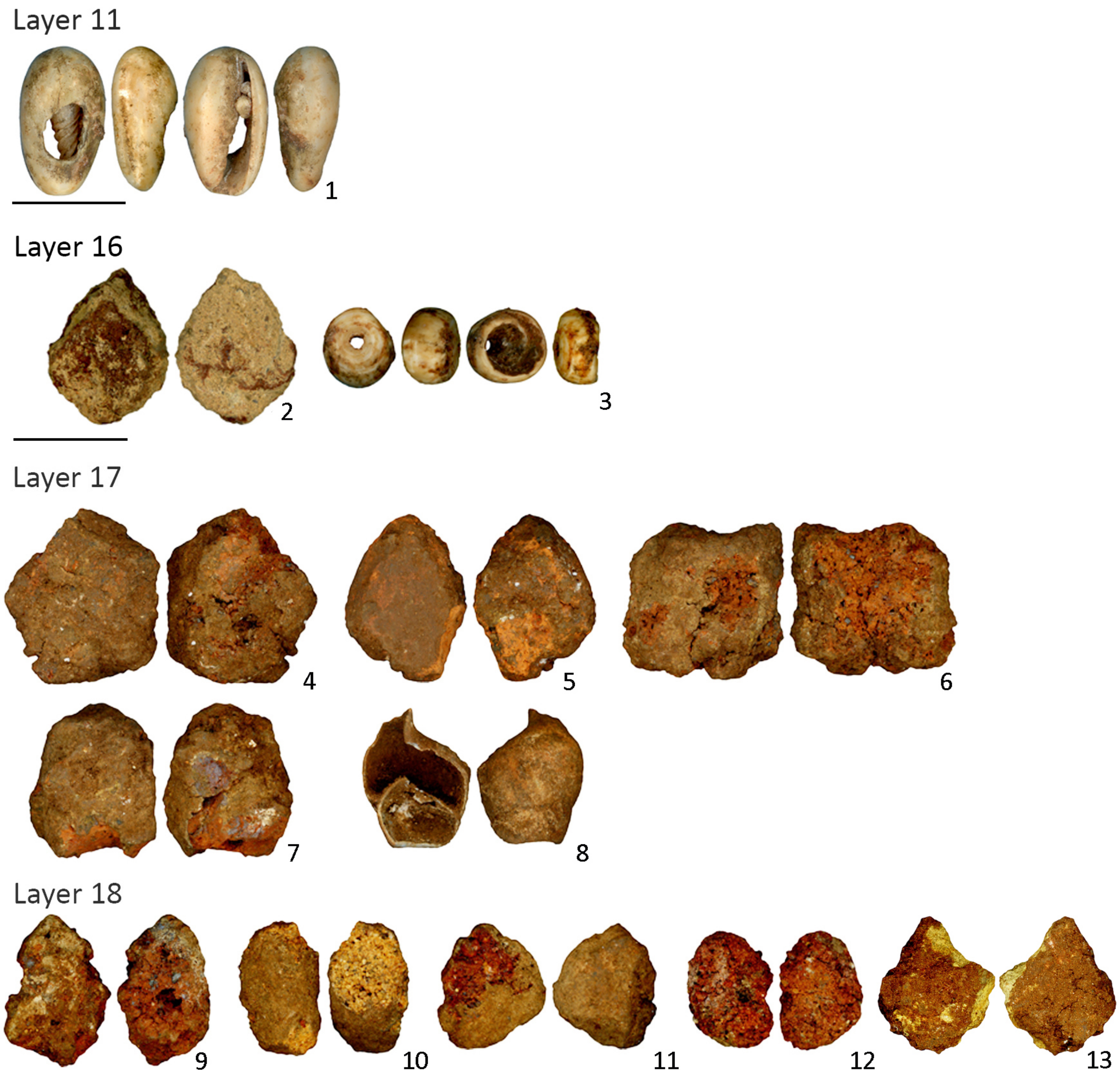
Layer 11
1
Layer 16
2
3
Layer 17
4
5
6
7
8
Layer 18
9
10
11
12
13


Type A
Type B
Type C
Type D
Type E
Type F

Trajectories of Middle to Later Stone Age cultural innovation in eastern Africa: the case of Panga ya Saidi, Kenya

Supplementary data

Figures S1-S25

Figure S1. Top: Spiral fragments of *Conus* shells from Layer 9 (context 413, spit B (left) and spit C (center and right)). Bottom: comparable fragments from thanatocoenoses obtained from Southern African shores. Scale = 1mm.

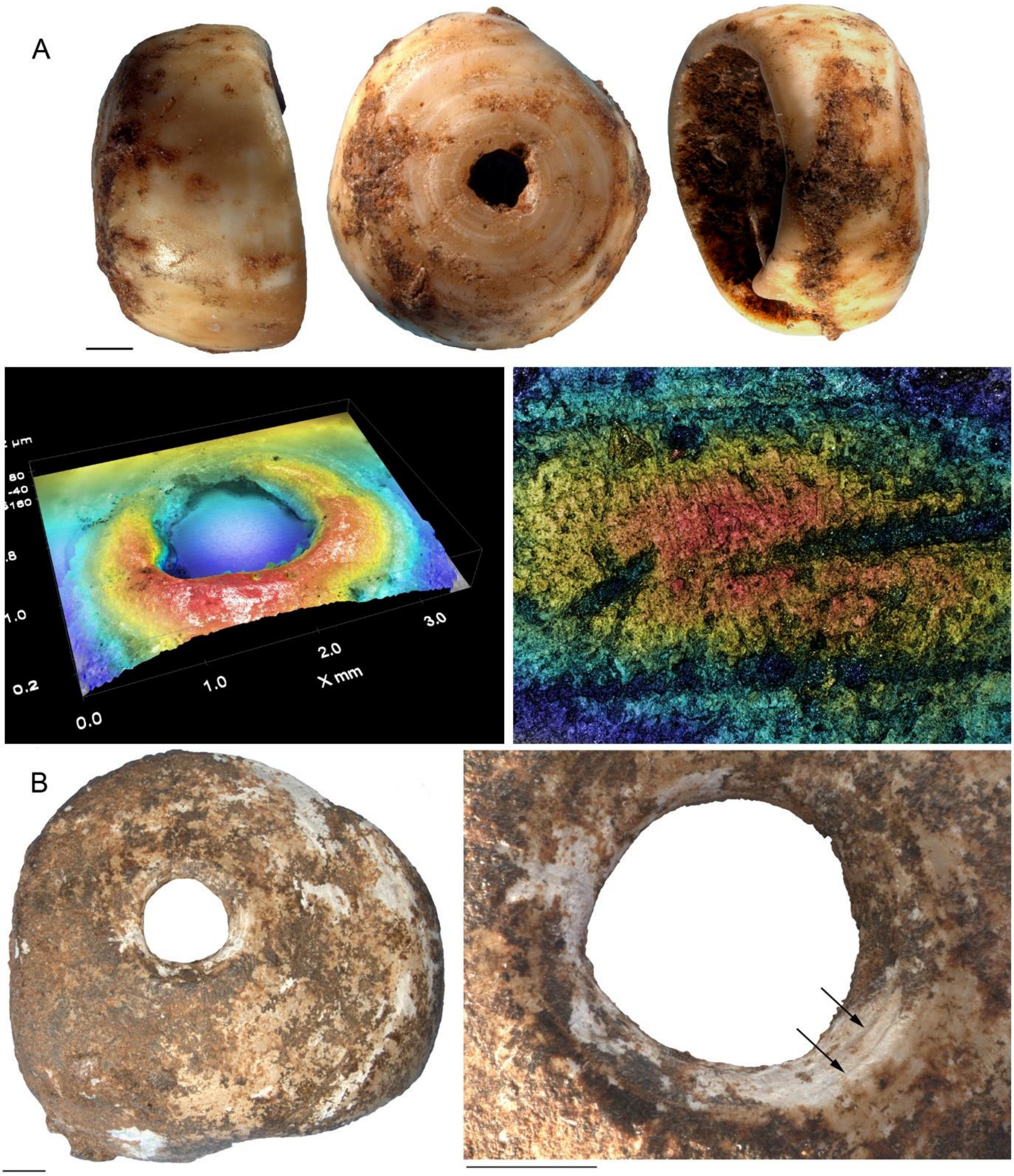

Figure S2. A: *Conus* shell from Layer 16 (context 420); Center: 3D reconstruction of the perforation (left), and an area close to the perforation showing horizontal grooves produced by coarse abrasion partially obliterated by vertical striations resulting from polish (right). B: *Conus* shell from Layers 7-8 (context 104, spit H), with possible traces left by a tool used to enlarge the natural perforation. Scale = 1 mm.

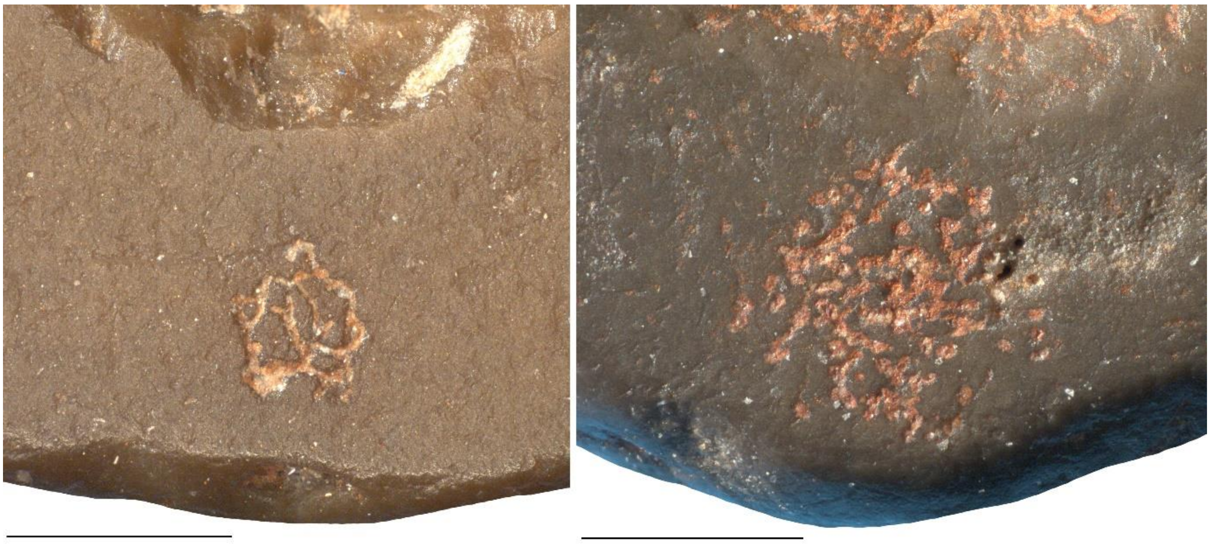

Figure S3. Close up-view of the ostrich egg shell outer face on OESB from Layers 7-8 (context 412). Variability in pore arrangements suggests the use of eggs of *Struthio camelus massaicus* (left) and *Struthio camelus molybdophanes* (right) (Schönwetter, 1927; Sauer, 1972). Scale = 1 mm.

Figure S4. A and B: OESB from Layer 5 (context 104, spit F) (A), and Layer 3 (context 408, spit A); B: with traces of abrasion; C: OESB from Layer 2 (context 102, spit B), showing polishing of the mammillary layer; D: OESB from Layer 7-8 (context 412), preserving traces of rotation on the perforation edge. Scale = 1 mm

Figure S5. Examples of OESBs not falling in any of the six main OESB types. A, B, C and D are from Layer 7-8 (context 412); E and F are from Layer 5 (context 104, spit F); G is from Layer 2 (context 102, spit B); H is from Layer 4 (context 408, spit B). Scale = 1 mm.

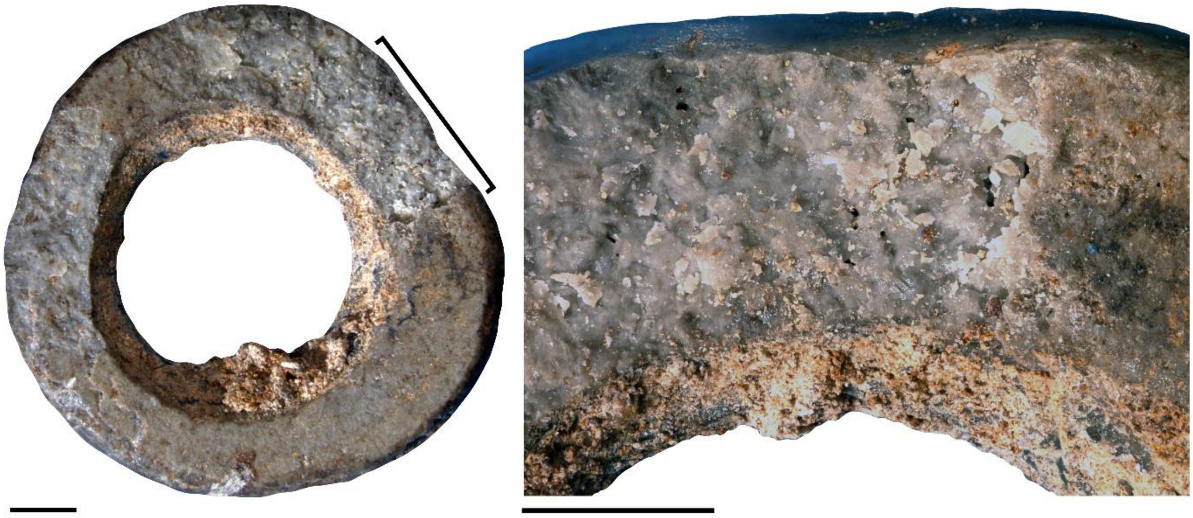

Figure S6. OESB from Layer 7-8 (context 412) showing removal of a large portion of the outer egg shell surface due to heating. Scale = 1 mm.

Figure S7. OESB from Layer 7-8 (context 412) exhibiting a thick red residue on the surface of the perforation. Scale = 1 mm.

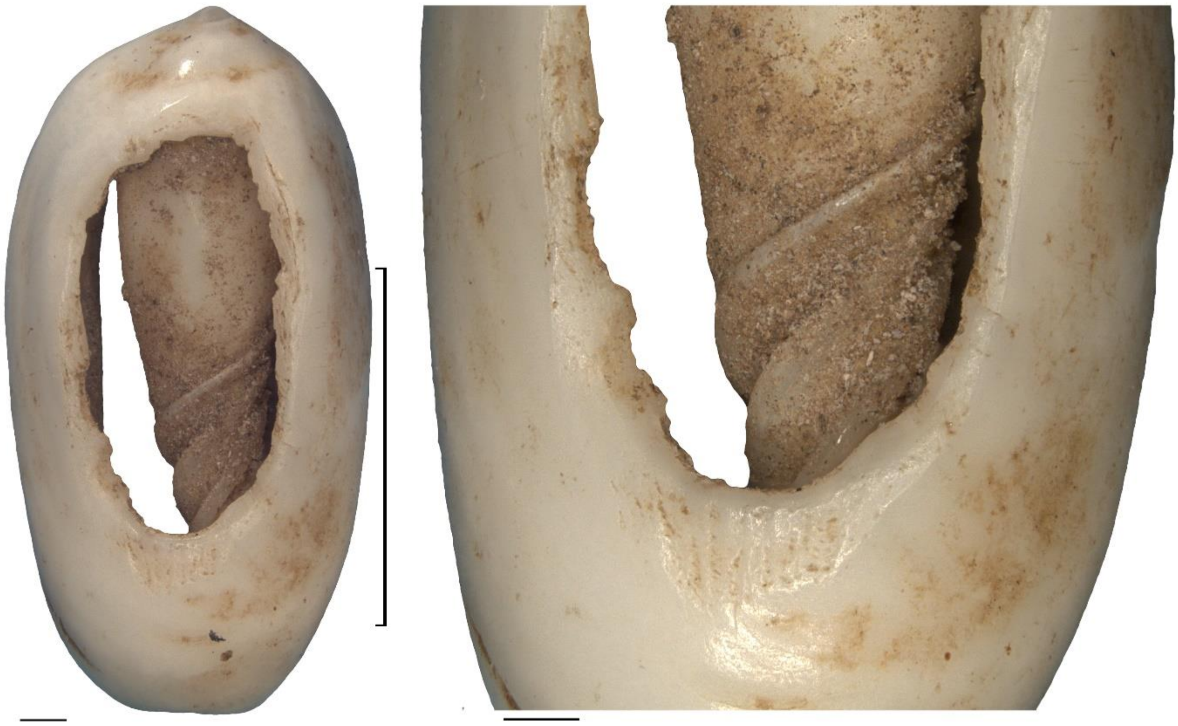

Figure S8. *Volvarina* sp. shell from Layer 4 (con

text 408, spit A), showing an elongated perforation enlarged by pressure. Scale = 1 mm.

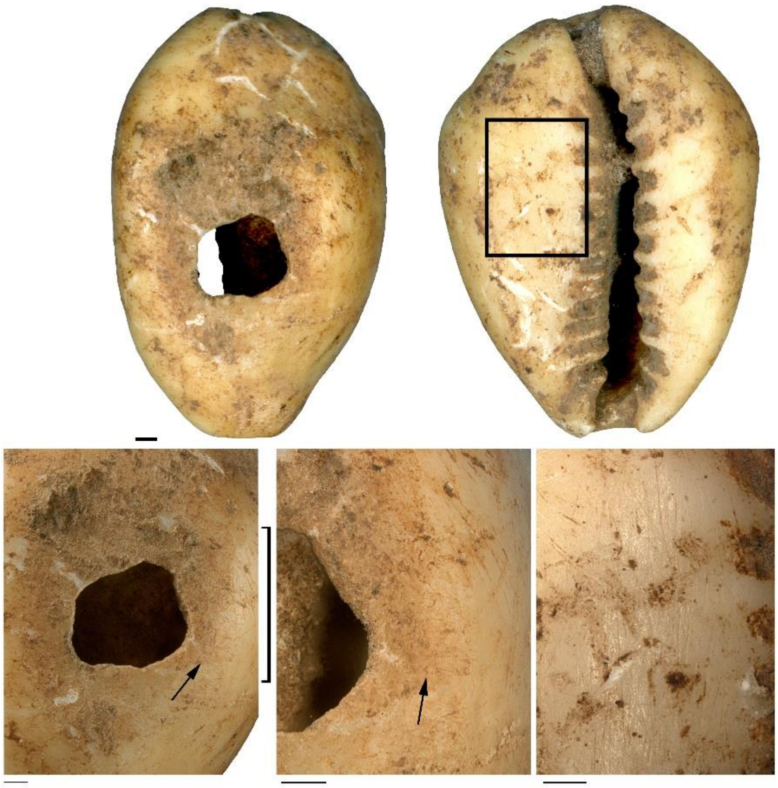

Figure S9. Top: *Cypraea moneta* from Layer 2 (context 407); bottom left and center: facet produced by grinding the body whorl surface in different direction before punching it in the middle; bottom right: subparallel striations produced by abrading the inner lip along the shell long axis. Scale = 1 mm.

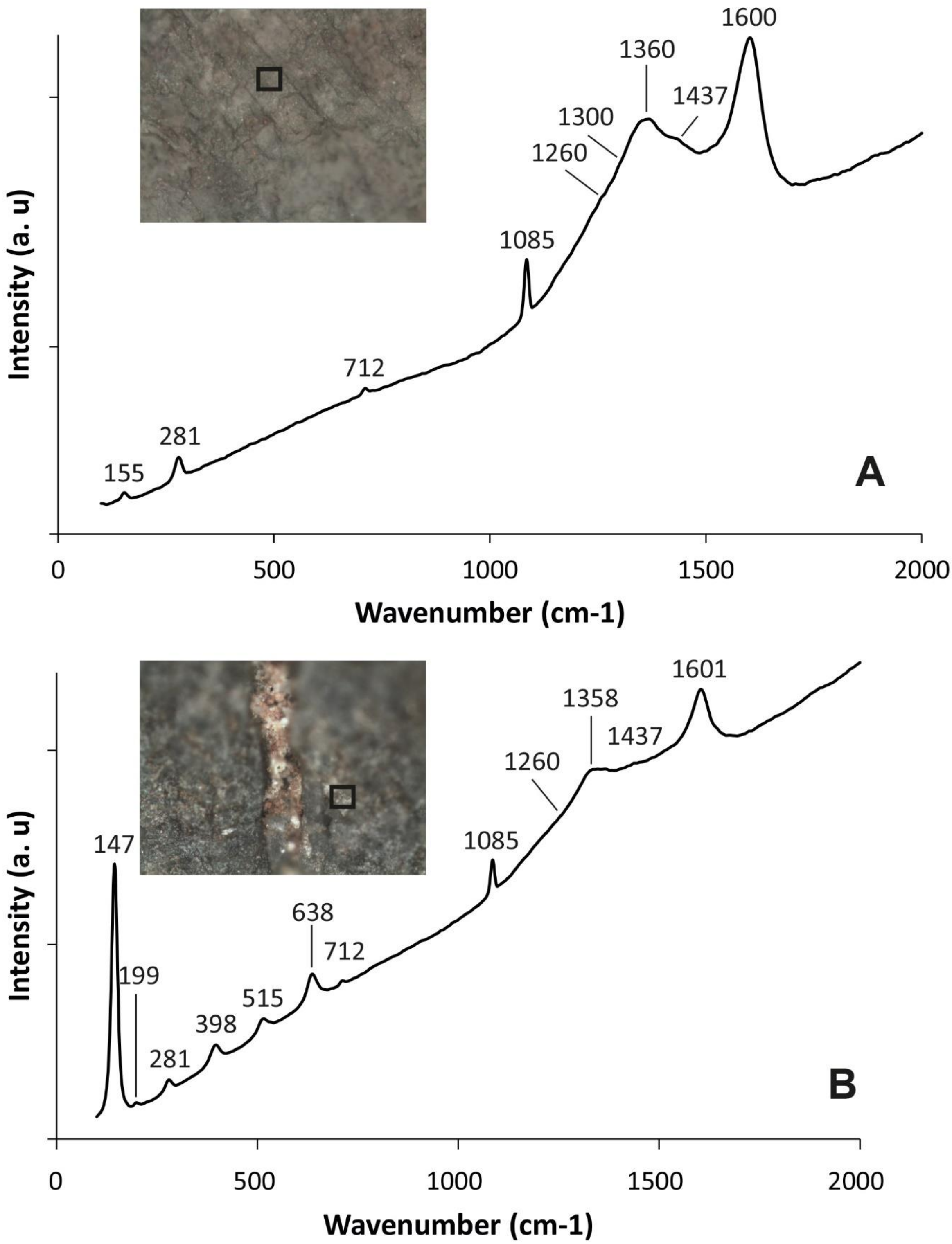

Figure S10. μ-RS spectra on black beads from Layer 3 (context 408, spit C). A, see Figure 1, n. 39; B, see Figure 1, n. 40.

Figure S11. A-B: marine shell beads from Layers 1-2 (context 402) (A), and Layer 3 (context 408, spit A) bearing cylindrical perforations and striations produced by flattening the bead surface. C: marine shell bead from Layer 3 (context 408, spit A), with an off-centre ovoidal perforation. B and C show remnant of bivalve sculpture. Scale = 1 mm.

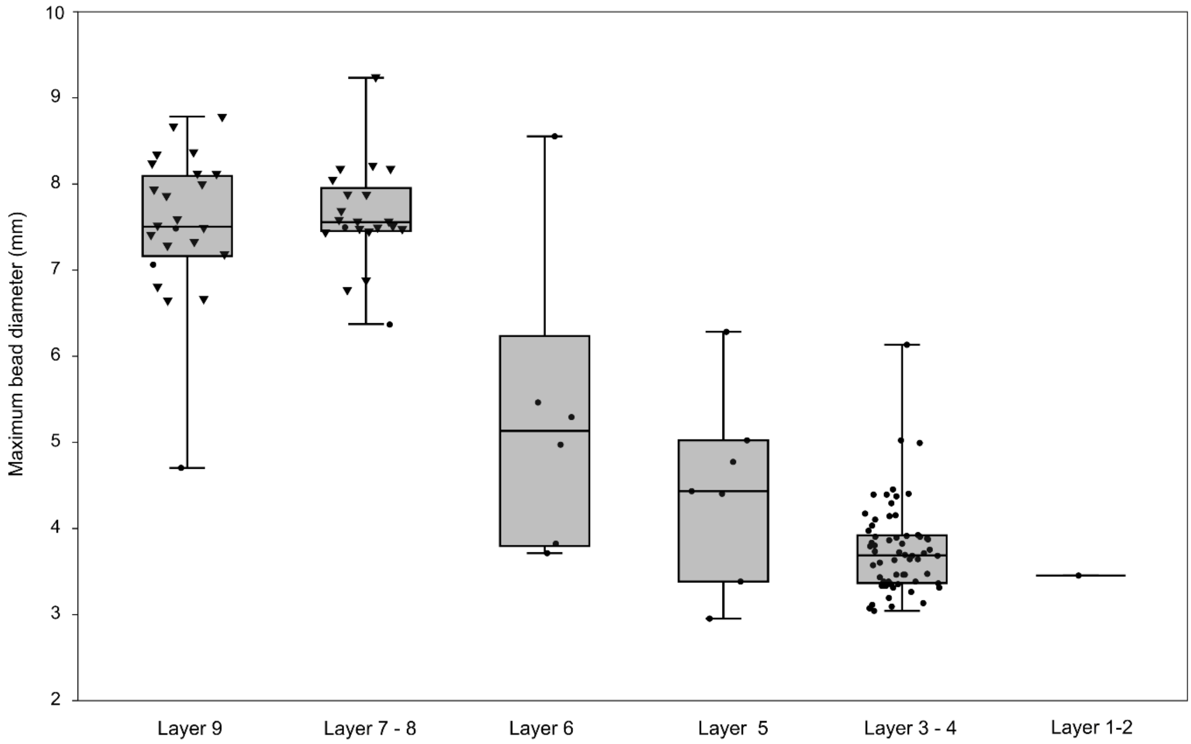

Figure S12. Stratigraphic variation in beads maximum diameter.

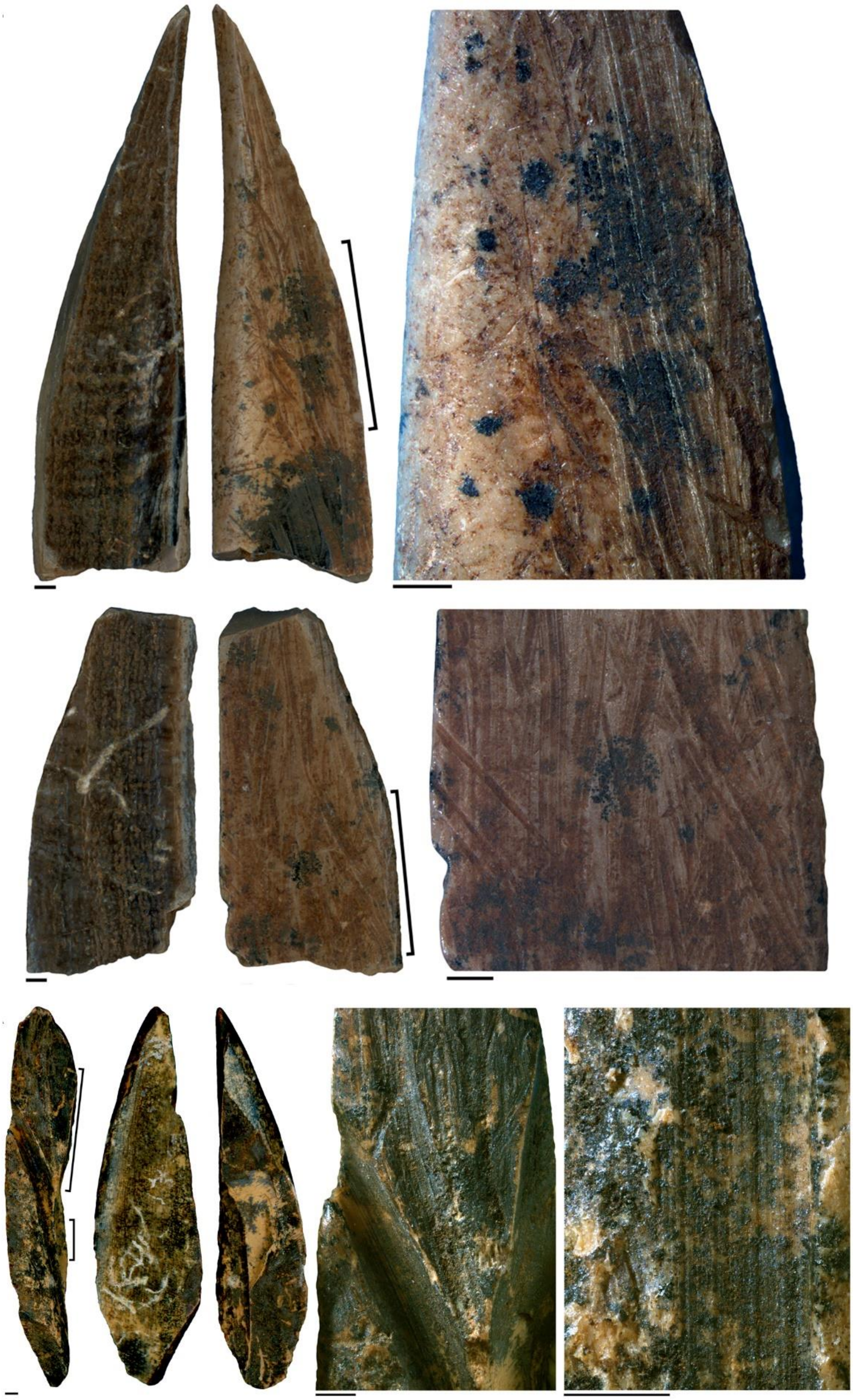

Figure S13. Top and centre: fragments of warthog or bushpig tusks from Layer 10 (context 414, spit D) showing scraping marks; bottom: fragment from Layer 7-8 (context 412) showing scraping marks and a deep groove. Scale = 1 mm.

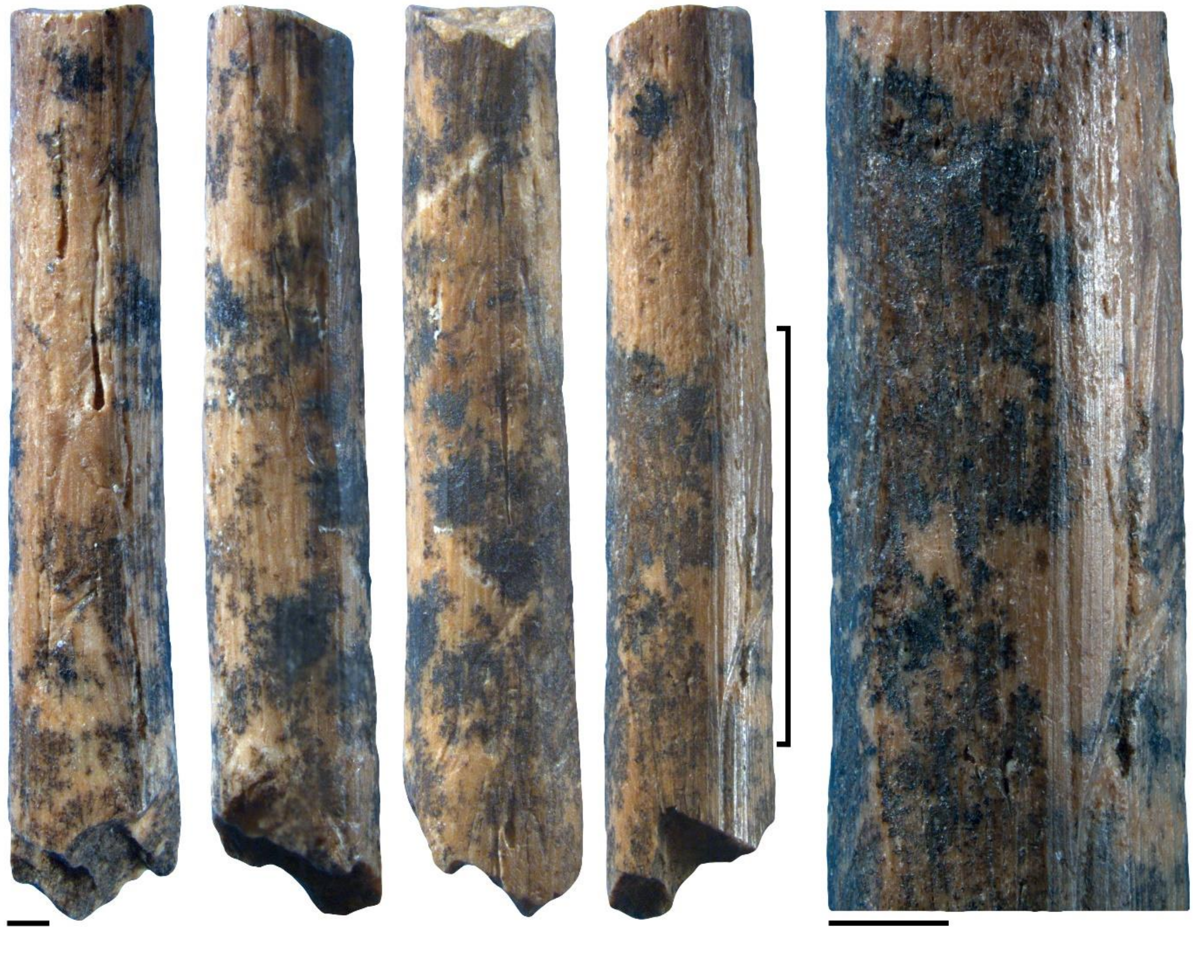

Figure S14. Mesial fragment of a bone point from Layer 9 (context 413, spit C), showing longitudinal scraping (close-up view at the right). Scale = 1 mm.

Figure S15. Notched bone fragments from Layer 9 (context 413, spit A). Scale = 1 mm.

Figure S16. Mesial fragment of a belemnite rostrum from Layer 9 (context 413, spit C), showing traces of abrasion (close-up on the right)). Scale = 1 mm.

Figure S17. Iron-rich nodule from Layer 8 (context 104, spit H) presenting a variety of modification traces (see text).

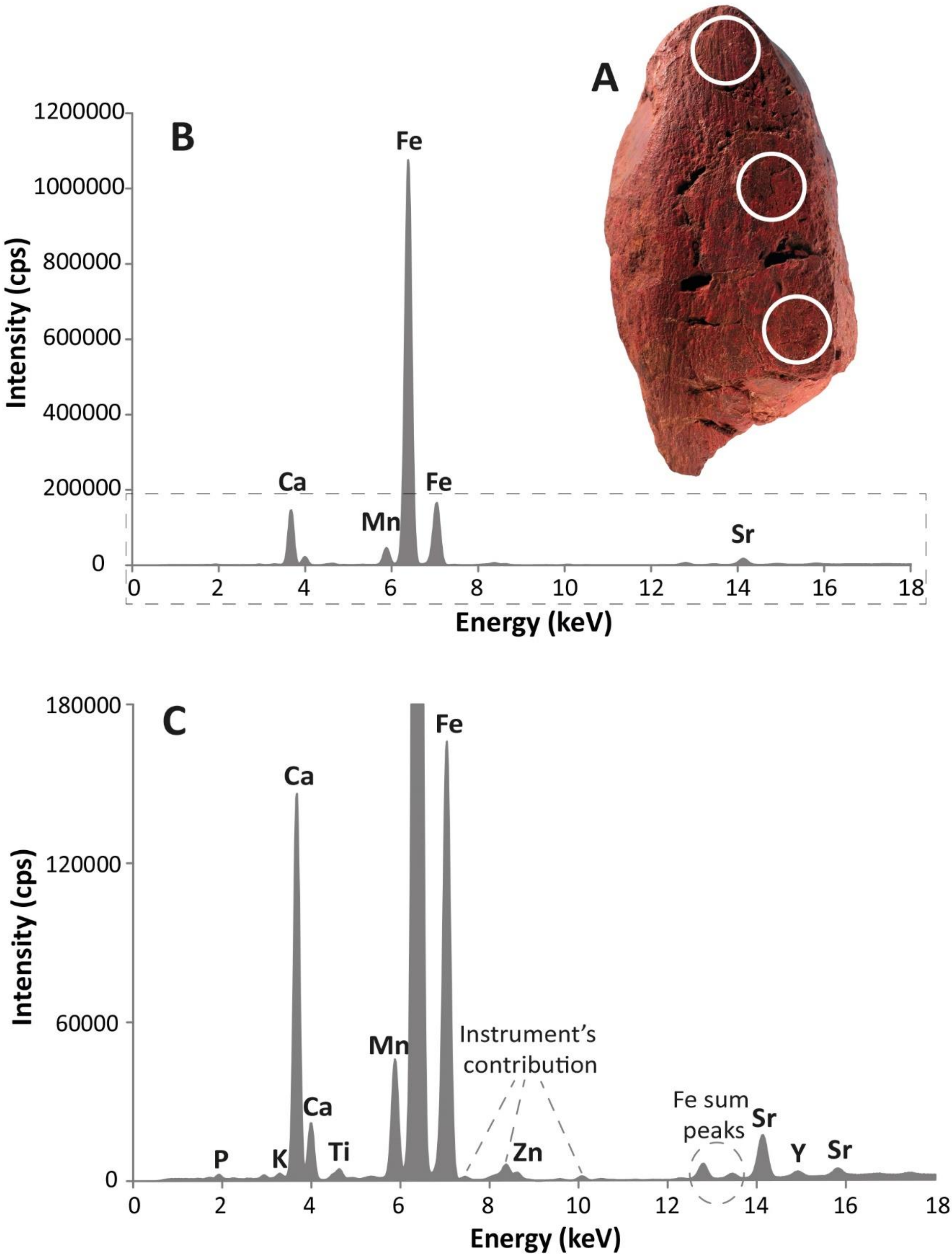

Figure S18. Result of the EDXRF analysis of the Iron-rich nodule from Layer 8 (context 104, spit H) within the specimen from Layer 10, context 313, spit P. A: Location of the analyses. B: EDXRF spectrum. C: Detailed view of the spectrum.

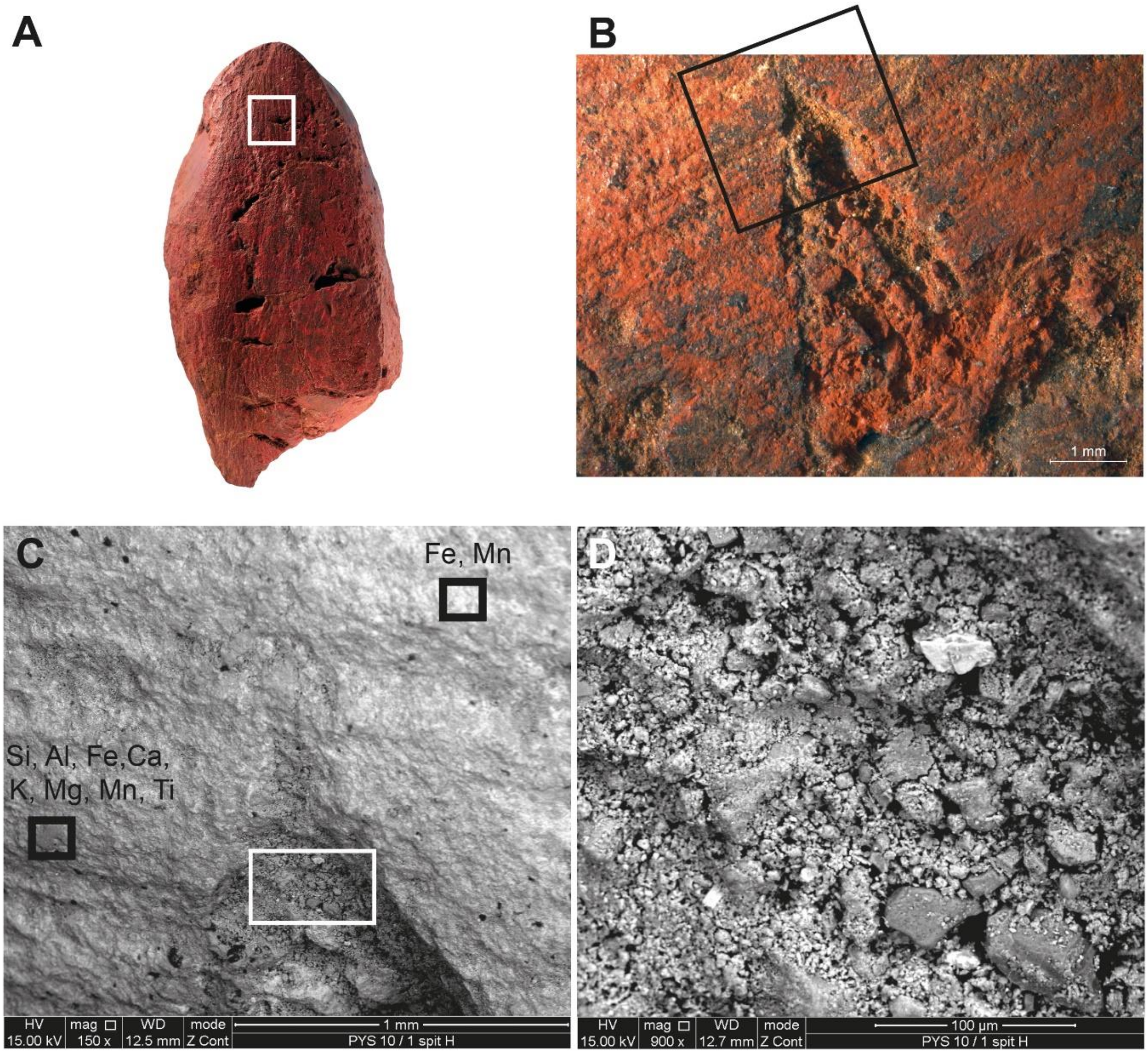

Figure S19. SEM-EDS analysis on the specimen from Layer 8 (context 104, spit H). A-B: Location of the analysis. C: Detailed view of B in BSE mode. D: Detailed view of C.

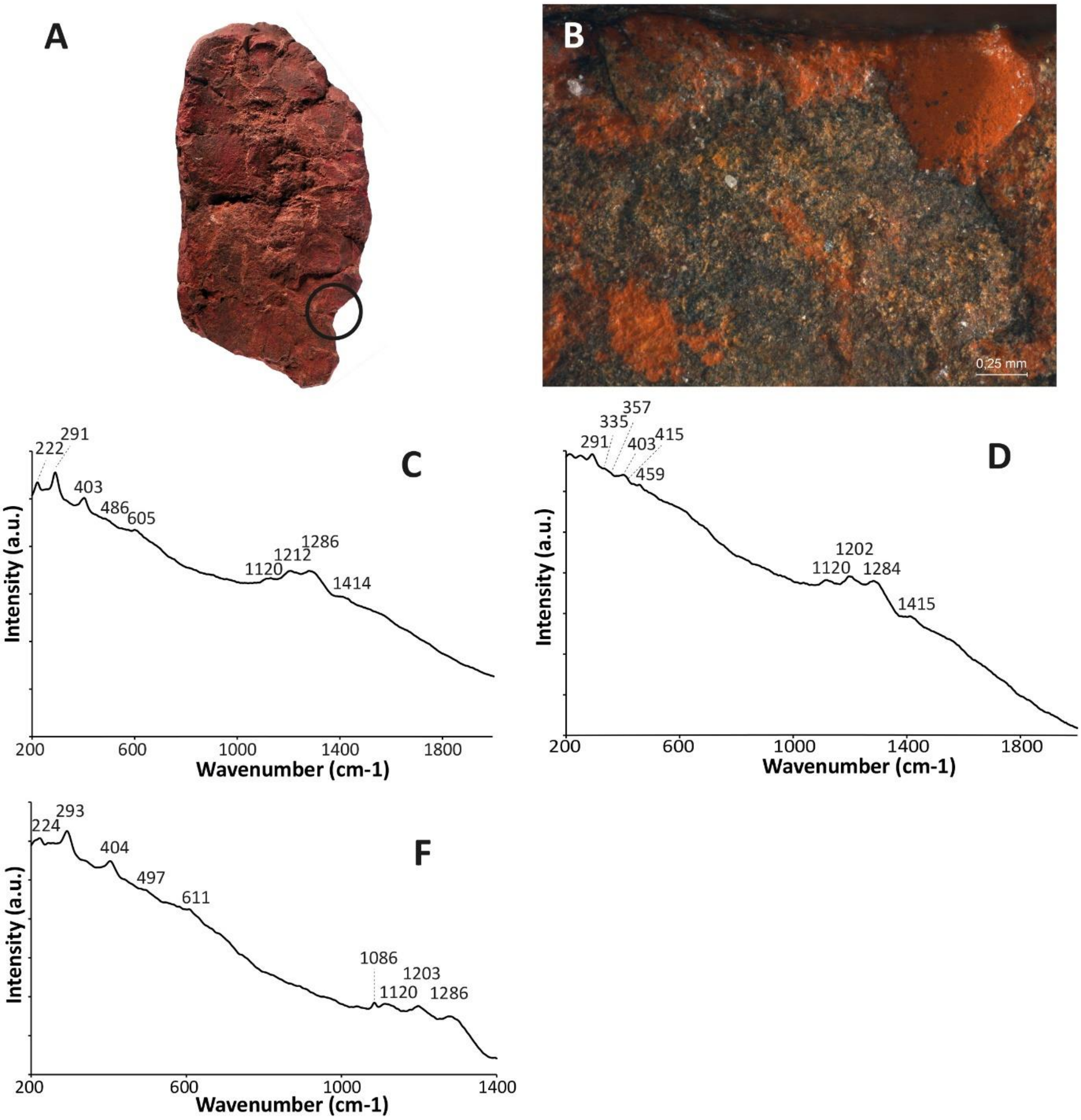

Figure S20. μ-RS analyses on the specimen from Layer 8 (context 104, spit H). A-B: Location of the analyses. C-E: Raman spectra of different sub-areas.

Figure S21. Engraved fragment of ochre from Layer 10 (context 313, spit P).

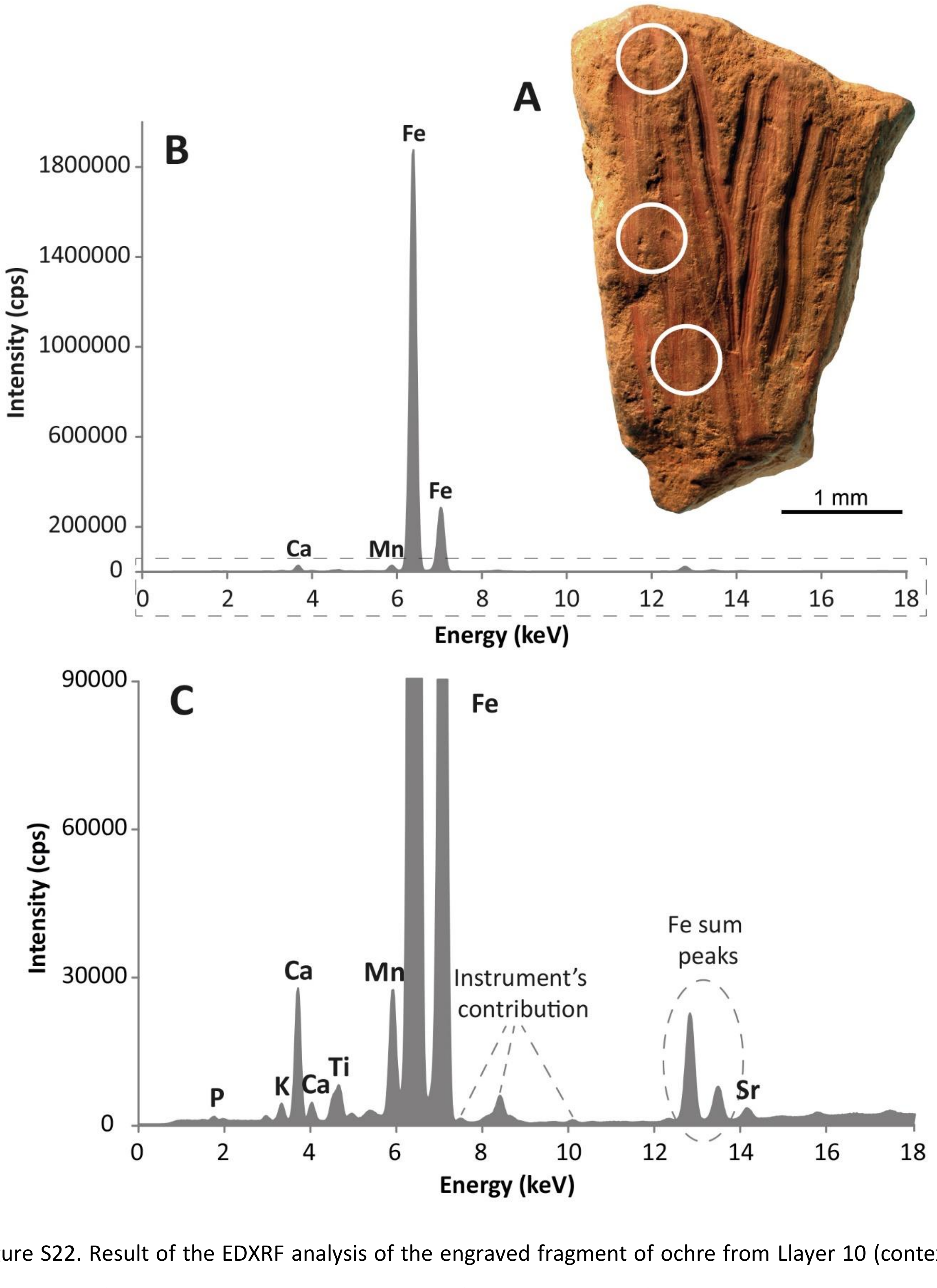

Figure S22. Result of the EDXRF analysis of the engraved fragment of ochre from Llayer 10 (context 313, spit P) within the specimen from Layer 10 (context 313, spit P). A: Location of the analyses. B: EDXRF spectrum. C: Detailed view of the spectrum.

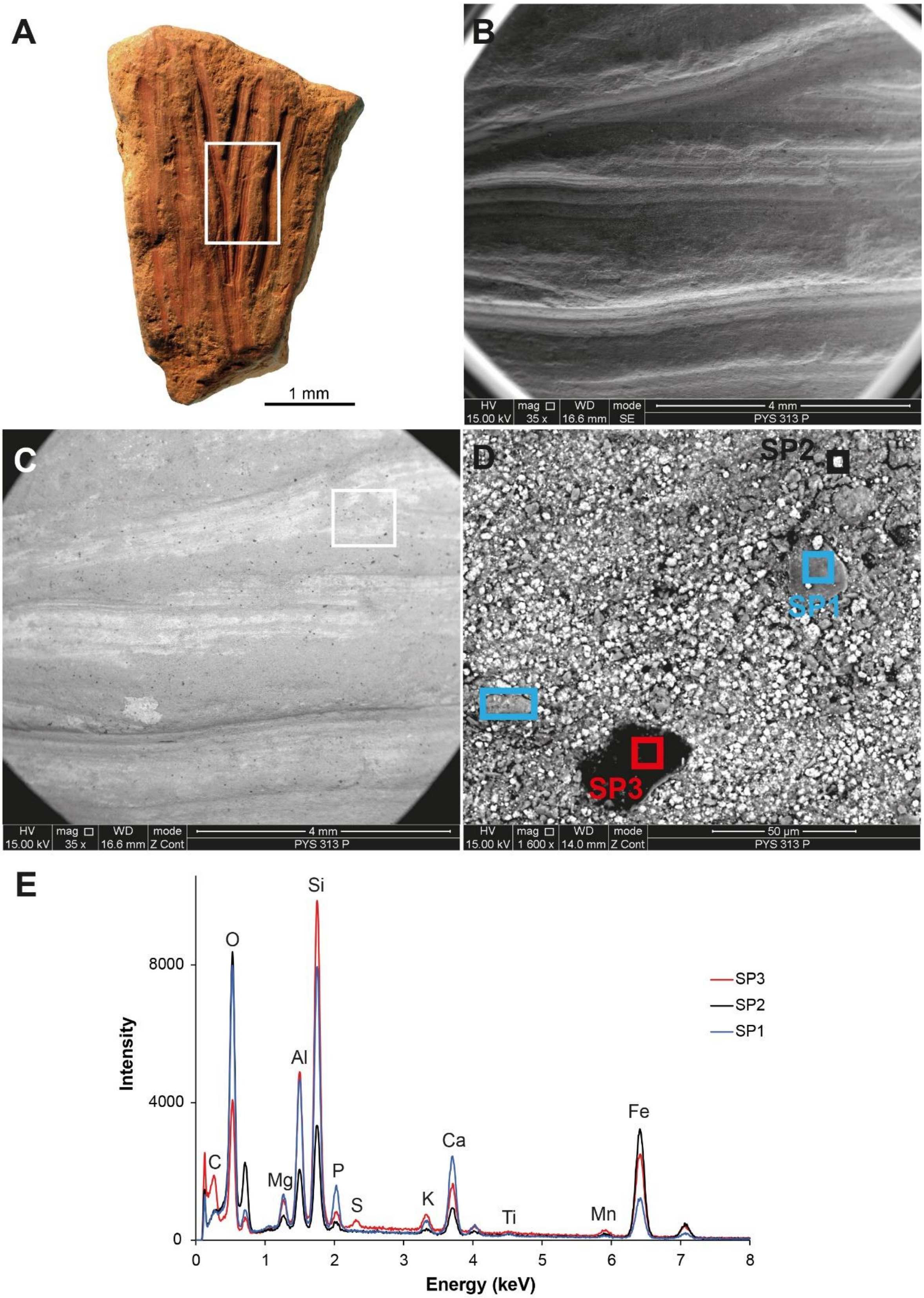

Figure S23. SEM-EDS analysis on the engraved fragment of ochre from Layer 10 (context 313, spit P). A: Location of the analyses. B-C: SE and BSE mode images at a low magnification. D: Detailed view in BSE mode with the location of the analyzed spots. E: EDS spectra.

A

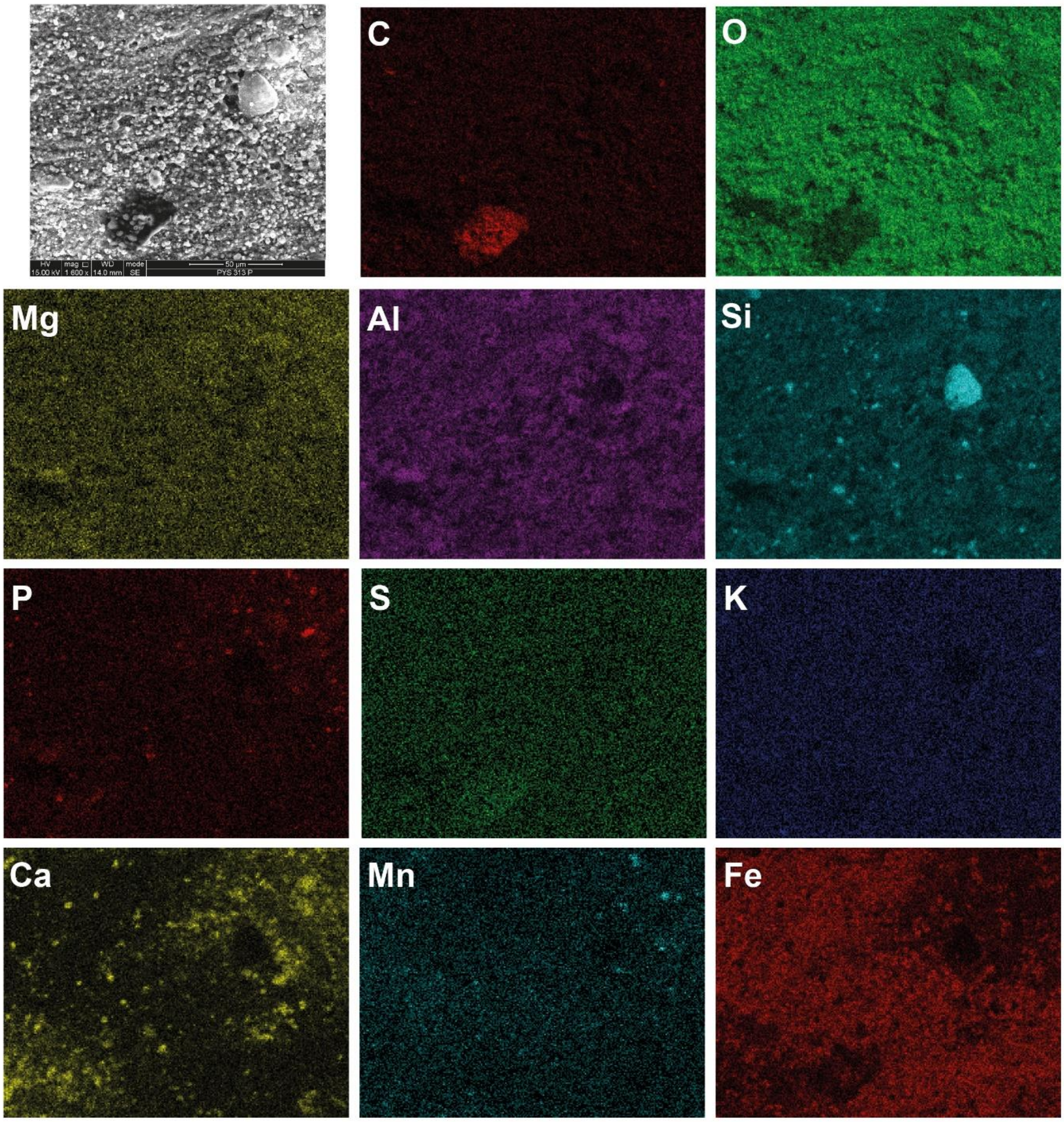

Figure S24. SEM-EDS analysis of the engraved fragment of ochre from Layer 10 (context 313, spit P). Distribution of the main elements composing the analyzed area.

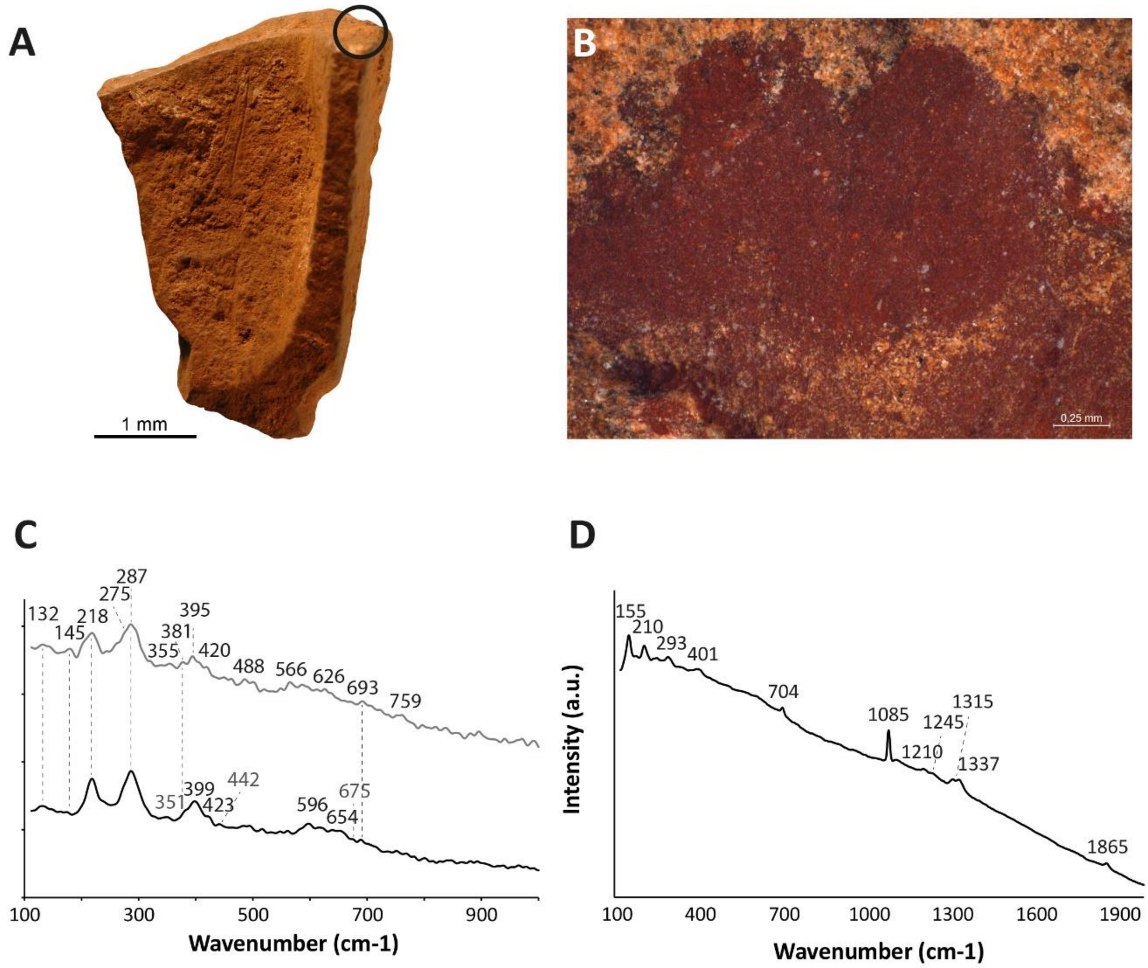

Figure S25. μ-RS analyses on the specimen from Layer 10 (context 313, spit P). A-B: Location of the analyses. C-D: Raman spectra of different compounds.

Trajectories of Middle to Later Stone Age cultural innovation in eastern Africa: the case of Panga ya Saidi, Kenya

Supplementary data

S Tables

Table S1. Contextual data and results concerning the pigment analyses.

Table S2. Results of μ-RS analyses on iron-rich lumps from PYS.

Table S3. Results of semi-quantitative SEM-EDS analysis of modified ochre lump PYS-Layer10-Context 313P.

Table S1. Contextual data and results concerning the pigment analyses

Unit	Layer	Context or Spit	Sub-sample	Color	Texture	Minerals (μ-RS)
III	7-8	412	a-b	Red	Laminated; clayish matrix with translucent grains (~25-150μm); presence of yellow nodules	hem, goe, qtz, cal, gyp
III	8	H (*)		Dark red	Compact clayish matrix	hem, undet. Mn compound, qtz, cal, sil
III	10	313 P (*)		Dark red	Compact clayish matrix	hem, qtz, cal, sil
III	10	414GNRL	b	Dark orange - bright red	Clayish matrix with some quartz grains (~200μm) randomly distributed within it; presence of black nodules	qtz, cal (**)
III	10	414D		Pale yellow	Grain-supported fabric composed of subrounded translucent grains (~60-120μm) in a clayish matrix	cal, undet. Sil (**)
II	16	420A		Yellow - dark red	Lump of hardened sediment with layers	(***)
I	17	420 F	a	Bright orange	Silty matrix with some angular quartz grains (~200μm) scattered on it; presence of vacuoles fulfilled with black deposits	hem, qtz
I	17	420 F	c	Dark orange - bright red	Concretioned silty matrix; grain-supported fabric composed of translucent rounded grains (~400μm) and black nodules (~600μm)	hem, undet. Mn compound, qtz
I	17	420 F	d	Dark orange - bright red	Concretioned silty matrix; grain-supported fabric composed of translucent rounded grains (~400μm) and black nodules (~600μm)	
I	17	420 F	e	Dark orange - bright red	Concretioned silty matrix; grain-supported fabric composed of translucent rounded grains (~400μm) and black nodules (~600μm)	hem, undet. Mn compound, qtz
I	18	422B	a	Dark orange - bright red	Concretioned silty matrix; grain-supported fabric composed of translucent rounded grains (~400μm) and black nodules (~600μm)	
I	18	422B	b	Dark orange - bright red	Concretioned silty matrix; grain-supported fabric composed of translucent rounded grains (~400μm) and black nodules (~600μm)	hem, qtz, cal
I	18	422B	d	Dark orange	Concretioned silty matrix containing translucent rounded grains (~200-300μm), white crystals (150μm), and white nodules; black impregnations are also present	hem, undet. Mn compound, qtz, pho
I	18	422B	e	Dark yellow - bright orange	Silty matrix; matrix-supported fabric; presence of subrounded translucent grains (~350-350μm); black impregnations are also present	hem, qtz, fel (**)

hem: hematite; goe: goethite; qtz: quartz; cal: calcite; gyp: gypsum; sil: silicates; pho: phosphates; fel: feldspar; (*) pieces with traces of human modification; (**) too intense fluorescence background; (***) no response

Table S2. Results of μ-RS analyses on iron-rich lumps from Panga ya Saidi						
Unit	Layer	Context or Spit	Sub-sample	Item analyzed	Identified minerals	N. meas.
III	8	H		Orange grains	hem (+ sil)	1
III	8	H		Red grains	hem (+ sil)	3
III	8	H		Dark red grains	hem (+ sil)	2
III	8	H		Black grains	undet. Mn compound	2
III	8	H		Translucent white crystals	cal (+ hem + sil)	1
III	8	H		Translucent white grains	qtz (+ hem)	1
III	7-8	412	a-b	Red grains	hem	4
III	7-8	412	a-b	Red grains	hem (+ cal + gyp)	1
III	7-8	412	a-b	Translucent white grains	qtz (+ hem)	2
III	7-8	412	a-b	Translucent white crystals	cal (+ goe + hem + gyp)	2
III	10	313 P		Orange grains	hem	1
III	10	313 P		Red grains	hem	3
III	10	313 P		Dark red grains	hem	3
III	10	313 P		Black grains	hem (+ qtz)	2
III	10	313 P		Translucent white crystals	cal (+ hem + sil)	1
III	10	313 P		Translucent white grains	qtz (+ hem)	2
III	10	414GNRL	b	Translucent white grains	qtz	2
III	10	414GNRL	b	Translucent grey crystals	cal	1
III	10	414D		Translucent grains surrounded by pale yellow particles	cal (+ undet. sil)	4
III	10	414D		Red grains	undet. compound	4
I	17	420 F	a	Red grains	hem (+ qtz)	2
I	17	420 F	c	Red grains	hem	3
I	17	420 F	c	Dark red grains	hem (+ undet. Mn compound)	1
I	17	420 F	c	Black grains	undet. Mn compound	6
I	17	420 F	e	Red grains	hem (+ qtz)	3
I	17	420 F	e	Black grains	undet. Mn compound (+ qtz)	1
I	18	422B	b	Red grains	hem	4
I	18	422B	b	Translucent white crystals	cal	2
I	18	422B	b	Translucent grey grains	qtz	3
I	18	422B	d	Red grains	hem	10
I	18	422B	d	Black grains	undet. Mn compound	4
I	18	422B	d	White particles	pho	1
I	18	422B	d	Translucent white grains	qtz	1
I	18	422B	e	Red grains	undet. compound	4
I	18	422B	e	Red grains	hem (+ alb)	2
I	18	422B	e	Translucent white grains	qtz (+ fel)	2

* in brackets associated minerals; meas: measurements; hem: hematite; sil: silicates; cal: calcite; qtz: quartz; gyp: gypsum; goe: goethite; pho: phosphates; alb; albite; fel: feldspar

Table S3. Results of semi-quantitative SEM-EDS analysis of modified ochre lump PYS-Layer10-Context 313P

Description			Items analyzed	Semi-quantitative EDX analyses **			Interpretation
Grain shape	**BSE * contrast**	**Grain size (µm)**		**>10%**	**2-10%**	**<2%**	
Irregular	Black	25	3	(Fe, Al, Si)	C (Ca)	S (Mn, Mg, K, P, Ti)	Undet.
-	Grey	Sub-micrometric	2	Fe, Si	Al, Ca, Mg	K, Mn, Ti (P)	Clay minerals
Rounded grains	Grey	2,5	1	Si (Fe)	(Al, Ca)	(K, Mg, P)	Quartz
Rounded tablets	Grey	20	2	(Fe) Si	(Al, Ca, P, Mg)	(K, Mn, Ti, Na)	Feldspars
Rounded grains	White	2,5	3	Fe	Si, Al, Ca	Mn, Mg, K, P	Hematite

(*): White, Grey, and Black refer to the contrast observed on backscattered electron (BSE) images; (**): Elements in brackets play no role in the mineralogical composition of the analyzed items.